Research Square

Preprints are preliminary reports that have not undergone peer review.
They should not be considered conclusive, used to inform clinical practice,
or referenced by the media as validated information.

Epilepsy-Associated GABRB3 Variants Differentially Alter Inhibitory Synapse Function and Nanoarchitecture

Dejan Gagoski
The University of Queensland Faculty of Health and Behavioural Sciences
Edmund Cotter
The University of Queensland Faculty of Health and Behavioural Sciences
Vincent L. Y. Loke
The University of Queensland School of Mathematics and Physics
Dubravka Skalamera
TRI: Translational Research Institute Australia
Pranesh Padmanabhan
The University of Queensland Faculty of Health and Behavioural Sciences
Justine Haddrill
The University of Queensland Faculty of Health and Behavioural Sciences
Li Xu
The University of Queensland Faculty of Health and Behavioural Sciences
Jingyi Wu
The University of Queensland Faculty of Health and Behavioural Sciences
Vincent Chen
The University of Queensland Faculty of Health and Behavioural Sciences
Joe W. Lynch
The University of Queensland Faculty of Health and Behavioural Sciences
Nela Durisic
n.durisic@uq.edu.au

The University of Queensland Faculty of Health and Behavioural Sciences https://orcid.org/0000-0002-7668-1039

Research Article

Keywords: GABRB3, Developmental and epileptic encephalopathy, GABAAR mobility and trafficking, Gephyrin, Synaptic nano-organization, Single-particle tracking

Posted Date: November 26th, 2026

DOI: https://doi.org/10.21203/rs.3.rs-11750792/v1

License: This work is licensed under a Creative Commons Attribution 4.0 International License.
Read Full License

Additional Declarations:
Table 1 is not available with this version

Title:

Epilepsy-Associated GABRB3 Variants Differentially Alter Inhibitory Synapse Function and Nanoarchitecture

Dejan Gagoski[1], Edmund Cotter[1], Vincent L. Y. Loke[1], Dubravka Skalamera[2], Pranesh Padmanabhan[3], Justine Haddrill[1], Li Xu[1], Jingyi Wu[1], Vincent Chen[1], Joe W. Lynch[1], and Nela Durisic[1],*

[1] Queensland Brain Institute, [2]Translational Research Institute, [3] School of Biomedical Sciences, Faculty of Health, Medicine and Behavioural Sciences, The University of Queensland, Brisbane, QLD 4072, Australia

* Correspondence: n.durisic@uq.edu.au

Abstract

Variants in GABRB3, encoding the β3 subunit of GABA-A receptors, are associated with epilepsy phenotypes ranging from childhood absence epilepsy to developmental and epileptic encephalopathies. To determine how disease severity relates to receptor and synaptic dysfunction, we compared the epilepsy-associated variants β3G32R and β3E180G using electrophysiology and single-molecule localisation-based imaging and tracking. β3G32R produced a partial loss of inhibitory synaptic function that was largely rescued by diazepam. β3E180G abolished detectable synaptic currents despite preserved surface expression and markedly increased surface receptor abundance in neurons, revealing a striking uncoupling between receptor localisation and inhibitory synaptic function. Beyond their effects on receptor function, the variants differentially altered inhibitory synapse organization. β3G32R increased synaptic receptor mobility and reduced synaptic dwell time, while β3E180G disrupted gephyrin organization, reduced active inhibitory synapses and dually innervated spines, and fragmented receptor nanodomains. Thus, progressively more severe receptor dysfunction was accompanied by progressively greater disruption of inhibitory synapse nano-organisation. These results highlight synaptic nanoarchitecture as an important contributor to disease severity, extending the pathogenic impact of $GABA_AR$ variants beyond receptor dysfunction alone.

Keywords:

GABRB3, Developmental and epileptic encephalopathy, $GABA_AR$ mobility and trafficking, Gephyrin, Synaptic nano-organization, Single-particle tracking

Abbreviations

CAE – Childhood absence epilepsy

DEE – Developmental and epileptic encephalopathy

DiS – Dually innervated spine

DZ – Diazepam

$GABA_AR$ – γ-Aminobutyric acid type A receptor

IPSC – Inhibitory postsynaptic current

SEP – Super-ecliptic pHluorin

uPAINT – Universal Point Accumulation Imaging in Nanoscale Topography

WT – Wild-type

SPT – Single-particle tracking

SMLM – Single-molecule localization microscopy

STORM – Stochastic optical reconstruction microscopy

HEK293 – Human embryonic kidney 293 cells

SEM – Standard error of the mean

ANOVA – Analysis of variance

Introduction

Epilepsy affects more than 50 million people worldwide and is one of the most common neurological disorders. Although epilepsies arise from diverse genetic and environmental causes, impaired inhibitory neurotransmission is a recurring pathogenic mechanism. Advances in genome and exome sequencing have identified numerous variants in genes encoding γ-aminobutyric acid type A receptors ($GABA_ARs$), establishing disrupted GABAergic signalling

as a major contributor to both common epilepsies and severe developmental and epileptic encephalopathies [1-4]. Despite the growing catalogue of disease-associated variants, the mechanisms linking receptor dysfunction to clinical severity remain incompletely understood.

Fast synaptic inhibition in the mammalian brain is mediated primarily by $GABA_AR$s, pentameric ligand-gated chloride channels assembled from combinations of α, β and γ subunits. The majority of synaptic $GABA_AR$s contain two α subunits, two β subunits and a γ2 subunit, although considerable diversity exists between brain regions and neuronal populations [5-7]. Inhibitory synaptic strength is not determined solely by receptor gating properties. Instead, it emerges from the interplay between receptor function, receptor abundance, synaptic dwell time and nanoscale organisation within the postsynaptic membrane. These parameters are regulated by dynamic interactions between $GABA_AR$s and the scaffold protein gephyrin, which controls receptor stabilisation and confinement at inhibitory synapses [8-10]. Consequently, disease-associated variants may compromise inhibition not only by altering channel function but also by disrupting the molecular organisation of inhibitory synapses.

Among $GABA_AR$ genes implicated in epilepsy, GABRB3, which encodes the β3 subunit, stands out because of the large number of pathogenic variants and the broad spectrum of associated phenotypes. Mutations in GABRB3 have been linked to childhood absence epilepsy, generalized epilepsy and severe developmental and epileptic encephalopathies including Lennox-Gastaut syndrome [4, 11, 12]. Functional studies *in vitro* and in mouse models have shown that many β3 variants impair receptor activity through altered gating, defective trafficking or reduced agonist responsiveness [1, 13, 14]. More recently, systematic analysis of GABRB3-associated epilepsies revealed that disease-causing variants segregate into gain-of-function and loss-of-function groups associated with distinct clinical phenotypes, demonstrating that the relationship between receptor dysfunction and disease severity is more complex than previously thought [1, 3]. However, most studies have focused on receptor pharmacology and biophysics, whereas much less is known about how pathogenic β3 variants affect receptor behaviour at inhibitory synapses, including receptor mobility, synaptic residence time and nanoscale organisation.

Recent advances in super-resolution microscopy have transformed our understanding of inhibitory synapses. Rather than forming homogeneous postsynaptic assemblies, gephyrin and $GABA_AR$s are organised into highly structured sub-synaptic domains that align with presynaptic neurotransmitter release sites [15-17]. This nanoscale architecture is increasingly

recognised as a major determinant of synaptic efficacy. Acute disruption of gephyrin organisation causes re-distribution of synaptic $GABA_ARs$ and impairs inhibitory transmission despite largely preserving receptor abundance, demonstrating that precise receptor positioning is critical for efficient synaptic signalling [9]. Single-particle tracking studies further show that receptor diffusion, trapping and synaptic dwell time directly influence inhibitory synaptic strength and plasticity [18-20]. Together, these findings raise the possibility that epilepsy-associated variants may impair inhibition not only by altering receptor function but also through remodelling of inhibitory synapse nanoarchitecture.

The β3 subunit is particularly relevant in this context because it contributes to both synaptic and extrasynaptic $GABA_AR$ populations and has been implicated in neuronal development, synaptogenesis, learning and memory [21-24]. Consistent with these roles, Gabrb3-deficient mice exhibit absence-like seizures, behavioural abnormalities and cognitive deficits [24-26]. Furthermore, recent high-resolution structures of native human $GABA_ARs$ have provided unprecedented insight into receptor composition and architecture, creating new opportunities to link epilepsy-associated mutations to receptor assembly, pharmacology and synaptic function [6, 23].

To determine whether molecular and synaptic dysfunction are associated with differences in clinical disease severity, we compared two epilepsy-associated β3 variants linked to disorders of markedly different severity. The β3G32R mutation is associated with childhood absence epilepsy, a relatively mild disorder with favourable developmental outcomes, whereas β3E180G has been identified in patients with Lennox-Gastaut syndrome, a severe developmental and epileptic encephalopathy [27, 28]. As shown in Fig. 1A, the two epilepsy-associated β3 variants occupy distinct structural environments within the extracellular domain. β3G32 is located near the N-terminus of the mature protein, whereas β3E180 lies within the GABA-binding pocket at the β3+/α1− interface in close proximity to bound GABA. Both residues are highly conserved across species (Fig. 1B), suggesting important structural and functional roles and supporting the pathogenicity of the G32R and E180G variants.

We generated a heterologous synapse preparation that allows direct electrophysiological analysis of recombinant $GABA_ARs$ with defined subunit composition. This approach enabled selective recording of inhibitory postsynaptic currents (IPSCs) mediated exclusively by receptors containing the mutant β3 subunits [20, 29-32]. The effects of each variant on receptor mobility and synapse nanoarchitecture were then examined in neurons using live-cell imaging,

single-particle tracking and super-resolution microscopy. Using this unique approach, we examined how these variants affect receptor function, trafficking, mobility and nanoscale organisation at inhibitory synapses. We further assessed their responsiveness to diazepam (DZ), a clinically relevant positive allosteric modulator of $GABA_A$Rs. We show that the two mutations produce distinct patterns of synaptic dysfunction, with the severity of receptor impairment mirrored by progressive disruption of inhibitory synapse nanoarchitecture. These findings identify synaptic remodelling as an important component of GABRB3-associated epilepsies and suggest that nanoscale organisation of inhibitory synapses may represent an important but previously unrecognised determinant of disease severity.

Results:

β3G32R impairs but β3E180G abolishes IPSCs

To determine how epilepsy-associated β3 variants affect synaptic inhibition, we examined IPSCs mediated by mutant $GABA_A$Rs. In neurons, $GABA_A$Rs contain a variety of subunits, which makes it difficult to distinguish the contribution of mutant-containing $GABA_A$Rs to the IPSCs. To circumvent this problem, we used hetero-synapse preparation for this set of experiments and generated synaptic contacts between neuronal presynaptic terminals and HEK293 cells expressing $GABA_A$Rs with predefined subunit composition [32-34]. By patching the HEK293 cells, we could selectively record IPSCs mediated by recombinant $GABA_A$Rs activated by GABA released from neuronal terminals [30, 31]. As α1 and γ2L are among the most abundant synaptic $GABA_A$R subunits in the brain [35], we first examined receptors composed of α1, γ2L, and either *wt* or mutant β3 subunits (Fig. 2). Cells expressing α1β3γ2L or α1β3G32Rγ2L receptors produced robust IPSCs, whereas α1β3E180Gγ2L receptors failed to generate detectable synaptic currents (Fig. 2A). Compared with *wt* receptors, β3G32R reduced iPSC amplitude by approximately 70% and accelerated current decay by approximately 25% (Fig. 2 B, C and Table S1).

Because β3 subunits can assemble into functional receptors lacking γ2, and β3G32R has previously been reported to affect receptor assembly [36], we next assessed whether mutant receptors incorporated γ2L. As expected, α1β3 receptors lacking γ2L generated significantly smaller currents with slower rise and decay kinetics than α1β3γ2L receptors (Fig. S1 and Table 1). In contrast, the kinetic properties of α1β3G32Rγ2L-mediated IPSCs remained clearly distinct from those of α1β3 receptors, suggesting that γ2L was incorporated into the majority of mutant receptors.

We next examined receptors containing the α5 subunit, which commonly co-assembles with β3 subunits and contributes to a slower component of GABAergic inhibition in several neuronal populations [35, 37-41]. Consistent with previous reports, α5β3γ2L receptors produced currents with slower rise and decay kinetics than α1β3γ2L receptors, while peak amplitudes were comparable (Fig. 2 D-F and Table S1). Introduction of β3G32R reduced iPSC amplitude and accelerated decay without affecting rise time, whereas β3E180G again abolished detectable synaptic currents. Similar to the α1-containing receptors, comparison with α5β3 receptors lacking γ2L indicated that γ2L incorporation was largely preserved in β3G32R-containing receptors (Fig. S1 and Table S1). Together, these findings indicate that β3G32R causes a partial loss of receptor function, whereas β3E180G abolishes synaptic $GABA_AR$ currents.

B3G32R and β3E180G do not alter $GABA_AR$ stoichiometry or surface expression in HEK293 cells

The absence of detectable synaptic currents from β3E180G-containing receptors could result from a severe functional deficit or impaired receptor trafficking. To distinguish between these possibilities, we quantified surface expression of β3 and γ2L subunits in HEK293 cells expressing α1- or α5-containing $GABA_ARs$ (Fig. 3). For these experiments, the extracellular N terminus of the β3 subunit was tagged with super-ecliptic GFP (SEP), allowing surface receptors to be detected in non-permeabilised cells using anti-GFP antibodies.

Robust surface expression of *wt* and mutant β3-containing receptors was observed under all conditions, as indicated by clear plasma membrane labelling (Fig. 3A). Quantification of fluorescence intensity revealed no significant differences in the surface expression of *wt* β3, β3G32R or β3E180G subunits in either α1- or α5-containing receptors. Likewise, γ2L fluorescence intensity was similar across all conditions, indicating that neither mutation affected γ2L incorporation into $GABA_ARs$ (Fig. 3B). Together, these results suggest that the functional deficits caused by β3G32R and β3E180G are not due to impaired receptor surface expression or altered γ2L incorporation. Notably, the complete loss of synaptic currents produced by β3E180G occurred despite robust surface expression of both β3 and γ2L subunits. These findings suggest that the primary defect caused by β3E180G reflects impaired receptor activation rather than defective receptor trafficking or assembly.

Diazepam restores the function β3G32RG-containing $GABA_ARs$ but not β3E180G

To determine whether the functional deficits caused by epilepsy-associated β3 variants could be rescued pharmacologically, we examined the effects of DZ, a positive allosteric modulator of $GABA_A$Rs. We first recorded IPSCs in extracellular solution and then applied 1 μM DZ to the same cell for 5 min, allowing direct comparison of control and drug-treated responses. Consistent with the experiments above, IPSCs were detected in cells expressing *wt* β3 or β3G32R-containing receptors but remained undetectable in cells expressing β3E180G (Fig. 4 A and B). In all cells expressing α1-containing $GABA_A$Rs, DZ increased IPSC amplitude and prolonged decay without affecting rise time in both *wt* and β3G32R receptors (Fig. S2A). Although DZ did not fully restore the amplitude of α1β3G32Rγ2L-mediated currents to *wt* levels shown in Fig. 2C and F, it prolonged current decay beyond that of *wt* receptors (Fig. 4C). To determine whether this potentiation compensated for the reduced peak current, we compared charge transfer through mutant receptors in the presence of DZ with *wt* receptors in control conditions. Both the cumulative probability distributions and the mean charge transfer per cell were indistinguishable between the two conditions, indicating that DZ restored net chloride flux through α1β3G32Rγ2L receptors (Fig. 4D). A similar effect was observed for α5-containing receptors. DZ increased charge transfer through α5β3G32Rγ2L receptors but did not completely restore their functional properties. In particular, the decay time constant remained approximately 35% shorter than that of *wt* α5β3γ2L receptors recorded in the absence of DZ (Fig. 4E). Despite the reduction in decay time constant, mean charge transfer following DZ treatment was not significantly different from that of *wt* receptors, although a trend toward lower values remained (Fig. 4F, Fig. S2B). Together, these results show that DZ effectively rescues the functional deficit caused by β3G32R, whereas β3E180G-containing receptors remain unresponsive to pharmacological potentiation.

The mutant β3 subunits alter gephyrin clustering at inhibitory synapses

To determine whether β3 variants affect the organisation of inhibitory synapses, we co-expressed pmCherry-gephyrin together with *wt* β3-SEP, β3G32R-SEP or β3E180G-SEP in cultured cortical neurons (Fig. 5A). Consistent with previous studies, β3-containing $GABA_A$Rs formed clusters that colocalised with gephyrin-positive inhibitory synapses, although extrasynaptic receptor clusters were also observed (Fig. 5A). Neither mutation altered the density of inhibitory synapses (Fig. 5B). However, expression of β3E180G was significantly higher than that of *wt* β3 or β3G32R, as measured from the SEP fluorescence signal (Fig. 5C).

Despite its elevated surface expression, β3E180G disrupted gephyrin organisation. Analysis of gephyrin puncta revealed a significant reduction in the average cluster area in neurons expressing β3E180G, whereas both β3 variants reduced the average fluorescence intensity of gephyrin clusters (Fig. 5D). Examination of the cluster size distributions showed a pronounced shift towards smaller gephyrin puncta in neurons expressing β3E180G (Fig. 5E), indicating a reduction in postsynaptic scaffold size.

Because gephyrin clustering depends on ongoing $GABA_AR$ activity, we next asked whether the changes observed with β3 variants could arise from impaired receptor function. To test this, cultured neurons were treated with the $GABA_AR$ antagonist Gabazine (10 μM, for 24 h), which blocks receptor activation and mimics the loss of $GABA_AR$ function. In untreated cultures, gephyrin cluster size was comparable to that observed in neurons expressing *wt* β3 subunits (Fig. 5 E and F). In contrast, Gabazine treatment shifted the distribution of gephyrin cluster sizes towards smaller values, closely resembling the phenotype observed with β3E180G expression. Gabazine also reduced both the average gephyrin cluster area and puncta intensity (Fig. 5 F to H). Together, these results suggest that prolonged impairment of $GABA_AR$ function destabilises gephyrin scaffolds and contributes to the reduction in inhibitory synapse size observed in neurons expressing epilepsy-associated β3 variants.

Epilepsy-Associated $GABA_AR$ Variants Differentially Alter Synaptic Receptor Mobility

Because the number and stability of $GABA_ARs$ at synapses are major determinants of inhibitory synaptic strength, we next examined whether the β3 variants affect receptor mobility at inhibitory synapses. To track individual surface receptors, we performed single-particle tracking using uPAINT in neurons expressing pmCherry-gephyrin together with *wt* β3SEP, β3G32R-SEP or β3E180G-SEP (Fig. 6A). Consistent with previous observations, $GABA_ARs$ diffused freely in extrasynaptic regions but became confined within gephyrin-positive synapses. Comparison of synaptic trajectories revealed that β3G32R-containing receptors were significantly more mobile than *wt* receptors, whereas β3E180G-containing receptors exhibited reduced mobility (Fig. 6B).

Closer inspection of receptor trajectories showed frequent transitions between freely diffusive and confined states as receptors entered or exited synaptic regions (Fig.6 C). Quantification of these events revealed that β3G32R increased receptor exchange at synapses, resulting in significantly more trapping and escaping events than observed for *wt* receptors (Fig. 6D). In

contrast, the behaviour of β3E180G-containing receptors was not significantly different from that of *wt* receptors.

We next examined receptor residence time at synapses. $GABA_A$Rs containing β3G32R displayed significantly shorter synaptic dwell times than *wt* receptors, whereas β3E180G did not affect receptor residence time (Fig. 6E). Analysis of receptor confinement showed that β3G32R increased the area explored by receptors within synapses, while β3E180G produced the opposite effect and restricted receptor movement to smaller synaptic regions (Fig. 6F).

Together, these results demonstrate that the two epilepsy-associated β3 variants alter synaptic receptor dynamics through distinct mechanisms: β3G32R destabilises synaptic $GABA_A$Rs by increasing receptor exchange and reducing synaptic residence time, whereas β3E180G enhances receptor confinement while reducing overall mobility.

$GABA_A$Rs containing β3G32R and β3E180G are organised differently at inhibitory synapses

In addition to measuring receptor mobility, uPAINT allowed us to reconstruct the nanoscale distribution of surface $GABA_A$Rs at inhibitory synapses. Representative images of neurons expressing *wt* β3SEP and pmCherry-gephyrin are shown in Fig. 7 A. Quantification of surface localisations revealed that neurons expressing β3G32R or β3E180G contained substantially higher numbers of surface receptors than neurons expressing *wt* β3, with approximately 5-fold and 10-fold increases in receptor density, respectively (Fig. 7B). However, when only gephyrin-associated receptors were considered, β3G32R-containing receptors were encountered at synapses more frequently than either *wt* or β3E180G-containing receptors. Strikingly, the marked increase in β3E180G surface receptor abundance contrasted with the complete absence of detectable synaptic currents observed in artificial synapse recordings. Thus, receptor abundance alone was not predictive of synaptic function, indicating that β3E180G uncouples surface receptor accumulation from effective inhibitory signalling.

To investigate synaptic receptor organisation, we analysed $GABA_A$R distributions using Voronoï tessellation. WT β3 and β3G32R receptors typically formed large synaptic receptor assemblies that were occasionally subdivided into smaller nanodomains. In contrast, β3E180G-containing receptors were more frequently partitioned into multiple small receptor clusters (Fig. 7C). Quantification of receptor localisation density at individual synapses (Fig. 7D) revealed that both β3 variants increased the number of receptor nanodomains relative to *wt* β3. However, the density of receptor localisations within these domains differed markedly between

the mutants, with β3G32R producing significantly denser receptor clusters than β3E180G. Detailed localisation-density distributions for individual synapses are shown in Fig. S3.

Given the severe functional deficit caused by β3E180G, we next examined whether this variant affected the number of active synaptic contacts. Active presynaptic terminals were identified using fluorescently labelled synaptotagmin-1 antibodies during live-cell imaging. Neurons expressing β3E180G exhibited approximately 30% fewer active synaptic contacts than neurons expressing *wt* β3 (Fig. 7D).

We also observed $GABA_AR$ clusters on dendritic spines, consistent with inhibitory synapses located on dually innervated spines (DiSs) (Fig. 7H). Quantification revealed that expression of β3E180G reduced the number of DiSs by approximately 50%, whereas β3G32R had no significant effect.

Together, these results demonstrate that β3E180G profoundly alters the nanoscale organisation of inhibitory synapses, reducing receptor clustering, active synapse number and inhibitory innervation of dendritic spines.

Discussion

In this study, we investigated how two epilepsy-associated GABRB3 variants linked to markedly different clinical phenotypes alter inhibitory synapse function and organisation. Using a combination of artificial synapses, single-molecule tracking and super-resolution imaging, we found that the β3G32R and β3E180G mutations produce distinct patterns of dysfunction extending beyond receptor biophysics. While β3G32R caused a partial loss of receptor function that could be largely compensated by DZ, β3E180G abolished detectable synaptic currents and profoundly altered inhibitory synapse organisation. Importantly, greater receptor dysfunction was accompanied by progressively larger alterations in gephyrin clustering, receptor mobility and nanoscale receptor organisation, suggesting that synaptic remodelling is an important component of GABRB3-associated epilepsies.

Previous studies of GABRB3 variants have primarily focused on receptor trafficking, agonist sensitivity and channel gating in heterologous systems [13, 27, 28, 42]. Consistent with these reports, we found that β3G32R reduced inhibitory synaptic currents whereas β3E180G produced an almost complete loss of receptor function. Surprisingly, however, neither mutation impaired receptor surface expression in HEK293 cells, indicating that the severe functional

deficit associated with β3E180G is unlikely to arise from defective trafficking alone. This is notable because many epilepsy-associated $GABA_AR$ mutations disrupt receptor biogenesis and surface delivery [3, 4, 12]. Instead, our findings suggest that β3E180G impairs GABA efficacy and channel gating sufficiently to prevent detectable synaptic signalling despite robust membrane expression. Indeed, one of the most unexpected findings was that β3E180G-containing receptors remained abundant at the cell surface despite producing no measurable synaptic currents. This dissociation between receptor abundance and receptor function indicates that β3E180G primarily affects receptor activation rather than receptor delivery to the plasma membrane. In this respect, β3E180G appears to uncouple surface receptor accumulation from inhibitory synaptic signalling. The preserved γ2L expression observed in our surface-labeling experiments further indicates that the mutation does not substantially impair receptor assembly or incorporation of the benzodiazepine-sensitive γ2 subunit.

An apparent discrepancy emerged between the heterologous and neuronal expression systems. Although β3E180G did not alter surface expression in HEK293 cells, neurons expressing β3E180G exhibited markedly elevated receptor abundance and surface localisation density. One possible explanation is that receptor trafficking and stabilisation are regulated differently in neurons, where interactions with endogenous scaffold proteins and activity-dependent pathways influence receptor turnover. Alternatively, the profound loss of receptor function may trigger compensatory accumulation of mutant receptors at the neuronal surface. Regardless of the mechanism, these findings indicate that synaptic dysfunction caused by β3E180G cannot be explained by impaired surface delivery alone.

Recent genotype-phenotype studies have demonstrated that GABRB3 variants segregate into gain-of-function and loss-of-function groups associated with distinct developmental and epileptic encephalopathy phenotypes [3, 13]. Our findings extend this framework by demonstrating that pathogenic variants differ not only in their effects on receptor function but also in their effects on inhibitory synapse organisation. Thus, the pathological consequences of GABRB3 mutations cannot be understood solely in terms of altered channel function. Instead, differences in receptor distribution, synaptic stability and nanoscale synaptic architecture are likely to represent additional determinants of disease severity [9, 24]. This may be particularly relevant for severe epileptic encephalopathies, where developmental impairment often exceeds what would be expected from altered receptor currents alone.

Several limitations should be considered when interpreting our findings. Although the artificial synapse system and receptor overexpression approaches do not fully recapitulate endogenous neuronal circuits, they enabled direct dissection of variant-specific effects on receptor function, mobility and nanoscale organisation. In addition, we focused on two representative GABRB3 variants spanning a broad range of clinical severity. Future studies in patient-derived neurons and animal models will be needed to determine the generality of these mechanisms across GABRB3-associated epilepsies and to establish how synaptic nanoarchitectural changes contribute to circuit dysfunction and disease progression. Nevertheless, the present findings identify synaptic nanoarchitecture as a previously overlooked dimension of GABRB3 pathophysiology.

One of the most striking findings of this study was the disruption of gephyrin organisation caused by β3E180G. Gephyrin is the principal scaffold protein responsible for anchoring $GABA_AR$s at inhibitory synapses and regulating receptor exchange between synaptic and extrasynaptic membrane compartments [10, 43, 44]. Although neither mutation altered inhibitory synapse density, β3E180G significantly reduced gephyrin cluster size and fluorescence intensity, indicating destabilisation of the postsynaptic scaffold. Importantly, prolonged pharmacological inhibition of $GABA_AR$ activity with Gabazine reproduced many aspects of this phenotype. This finding suggests that gephyrin remodelling is at least partly a consequence of reduced receptor activity rather than a direct structural effect of the mutation itself [10, 43]. Such bidirectional coupling between receptor activation and scaffold organisation is a well-established feature of inhibitory synapses and contributes to homeostatic regulation of synaptic efficacy [45].

The observed reduction in gephyrin cluster size is likely to have functional consequences beyond receptor anchoring. Previous studies demonstrated that alterations in gephyrin clustering are accompanied by corresponding changes in inhibitory postsynaptic current amplitude, indicating a close relationship between scaffold organisation and inhibitory synaptic strength [46, 47]. Similarly, inhibitory long-term potentiation is associated with increased gephyrin nanodomain density and nanoscale rearrangement of inhibitory postsynaptic densities without a corresponding increase in total synaptic area [10, 15]. Thus, the reduction in gephyrin clustering observed in β3E180G-expressing neurons would be expected to weaken inhibitory signalling independently of the primary receptor defect. Collectively, these observations suggest that defective receptor function and scaffold destabilisation act synergistically to impair inhibition.

The ability of chronic $GABA_AR$ blockade to mimic several aspects of the β3E180G phenotype further emphasises the bidirectional relationship between receptor activity and organisation of the inhibitory postsynaptic scaffold. Gephyrin clustering is dynamically regulated by phosphorylation- and palmitoylation-dependent signalling pathways downstream of receptor activation, while gephyrin itself stabilises receptors and regulates their confinement at synapses [43, 47]. We therefore propose that the profound loss of receptor function caused by β3E180G initiates a feedback process that progressively remodels inhibitory synapses, leading to reduced scaffold size, altered receptor organisation and impaired maintenance of inhibitory signalling. Such activity-dependent structural plasticity may represent an important but previously unrecognised mechanism through which severe epilepsy-causing mutations exert their effects over time.

Our single-particle tracking experiments further revealed that the two mutants altered receptor dynamics through distinct mechanisms. β3G32R increased receptor exchange at synapses, shortened synaptic dwell time and expanded the area explored by receptors within synaptic regions, indicating weaker receptor retention. Similar increases in $GABA_AR$ mobility have previously been reported in experimental epilepsy models and in neurons expressing epilepsy-associated $GABA_AR$ variants [48-50]. Taken together, these studies suggest that destabilisation of receptor trapping may represent a common mechanism contributing to disinhibition in epileptic networks. Reduced receptor dwell time would be expected to decrease occupancy of gephyrin binding sites and lower the likelihood that receptors are positioned optimally for activation during synaptic transmission.

In contrast, β3E180G reduced receptor mobility and increased confinement without significantly altering synaptic residence time. At first glance, this finding appears paradoxical given the profound functional deficit associated with this mutation. One potential explanation is that the elevated surface expression of β3E180G-containing receptors promotes molecular crowding within the plasma membrane. Experimental and computational studies have shown that increased membrane protein density can reduce lateral diffusion through steric hindrance and transient intermolecular interactions [51, 52]. Likewise, molecular crowding can enhance receptor confinement and limit exchange between synaptic and extrasynaptic pools [53, 54]. Although our experiments were not designed to directly test this mechanism, the combination of increased surface receptor density and reduced mobility is consistent with a contribution of crowding to the β3E180G phenotype. The elevated receptor abundance may also help explain why β3E180G receptors remain highly confined despite profound loss of function, further

supporting the idea that receptor organisation and receptor activity become uncoupled in the presence of this mutation. Alternatively, the mutation may strengthen receptor retention through prolonged interactions with residual scaffold elements, even in the context of disrupted synaptic organisation.

A further, non-mutually exclusive explanation involves altered conformational state dynamics. Recent studies indicate that $GABA_AR$ activation and desensitization regulate receptor diffusion and synaptic exchange, with activated or desensitized receptors undergoing lateral redistribution and replacement by resting receptors. If β3E180G severely impairs agonist-induced activation, mutant receptors may remain predominantly in a resting conformation and consequently fail to participate in normal activity-dependent exchange processes. Such a mechanism could reduce receptor turnover and promote confinement despite the marked loss of receptor function [50, 55].

Recent advances in super-resolution microscopy have revealed that inhibitory synapses possess highly organised nanoscale architectures consisting of receptor-rich nanodomains aligned with presynaptic release sites [9, 15-17]. Such organisation is increasingly recognised as a critical determinant of synaptic efficacy. Indeed, acute disruption of receptor nanoalignment can reduce inhibitory transmission without changing receptor number or intrinsic receptor function [9]. Our findings extend these observations by demonstrating that an epilepsy-associated $GABA_AR$ mutation can profoundly alter inhibitory synapse nanoarchitecture. Although both β3 variants increased compartmentalisation into subsynaptic domains, β3E180G generated smaller and less densely populated receptor assemblies, reduced the number of active synaptic contacts and decreased inhibitory innervation of dendritic spines. These findings indicate that the severe functional deficit associated with β3E180G is accompanied by structural remodelling that further compromises inhibitory signalling.

More broadly, our findings support the emerging view that neurodevelopmental disorders can arise not only from defects in receptor function but also from abnormalities in synaptic scaffolding and nanoscale synaptic organisation. Super-resolution studies have shown that inhibitory synapses are organised into dynamic nanoscale assemblies of $GABA_ARs$, gephyrin, adhesion molecules and associated signalling proteins, whose spatial organisation contributes to the efficacy and stability of synaptic inhibition. Disruption of these nanoscale architectures is increasingly recognised as a mechanism linking synaptic protein dysfunction to neurodevelopmental disorders, including intellectual disability, autism spectrum disorders and

epilepsy [16, 56]. Within this framework, β3E180G appears to behave not simply as a dysfunctional ion channel but as a mutation that disrupts the structural organisation of the inhibitory postsynaptic apparatus itself.

The reduction in dually innervated spines observed in β3E180G-expressing neurons may be particularly relevant to disease pathogenesis. Dually innervated spines provide highly localised inhibitory control of excitatory inputs and are increasingly recognised as important sites for synaptic integration and plasticity [57, 58]. Loss of inhibitory synapses at these structures would be expected to increase dendritic excitability and impair local regulation of excitation. Furthermore, the reduction in active synaptic contacts suggests that prolonged disruption of $GABA_AR$ signalling may affect maintenance of inhibitory connectivity. While our experiments do not establish causality, these observations are consistent with the notion that inhibitory neurotransmission contributes not only to synaptic function but also to long-term stabilisation of neuronal circuits.

Another important consideration is that synaptic efficacy is determined not only by receptor number or receptor function but also by their precise spatial relationship to neurotransmitter release sites. The concept that neurotransmitter receptors are organised into subsynaptic nanodomains aligned with presynaptic release machinery has emerged from studies of both excitatory and inhibitory synapses [9, 16, 59]. Consequently, alterations in receptor positioning caused by pathogenic mutations may substantially amplify the impact of primary channel defects. Our findings support this model by showing that the mutation associated with the most severe clinical phenotype also produces the greatest disruption of inhibitory synapse nanoarchitecture.

From a therapeutic perspective, our data provide evidence that the consequences of GABRB3 mutations depend strongly on the nature of the underlying molecular defect. DZ substantially increased charge transfer through β3G32R-containing receptors and largely compensated for the reduction in synaptic current amplitude. In contrast, β3E180G-containing receptors remained unresponsive. These findings are consistent with growing interest in precision therapeutic approaches for $GABA_AR$-associated epilepsies, in which variant-specific mechanisms may predict responsiveness to pharmacological intervention [13, 60]. More generally, our results suggest that preservation of residual receptor function may be a critical determinant of whether positive allosteric modulators remain effective. While benzodiazepines

may substantially improve inhibition mediated by partially functional receptors, they are unlikely to benefit receptors that have lost the capacity to respond to GABA.

In summary, we demonstrate that epilepsy-associated GABRB3 variants alter inhibitory neurotransmission through mechanisms that extend well beyond receptor gating. The relatively mild β3G32R variant primarily destabilises synaptic receptor retention and partially impairs receptor function, whereas the severe β3E180G variant abolishes inhibitory currents and drives extensive remodelling of inhibitory synapse nanoarchitecture. These observations support an emerging model in which differences in clinical severity may reflect not only the magnitude of receptor dysfunction but also the extent of disruption to inhibitory synapse organisation and dynamics. More broadly, our work identifies inhibitory synapse nanoarchitecture as an important mechanistic dimension of genetic epilepsy and suggests that disruption of nanoscale synaptic organisation may contribute substantially to the pathogenesis of developmental and epileptic encephalopathies.

Experimental model and subject details

Animals

All animal procedures were performed in accordance with institutional and national guidelines and were approved by the University of Queensland Animal Ethics Committee.

HEK293 cell culture

HEK293 cells (Thermo Fisher Scientific, R70507) were maintained in DMEM supplemented with 10% foetal bovine serum at 37°C in a humidified incubator containing 5% CO_2.

Primary neuronal cultures

Primary cortical neuronal cultures were prepared from embryonic day 18 (E18) Wistar rat embryos of either sex as previously described [61]. Cortical tissue was dissociated by trituration and resuspended in DMEM supplemented with 10% fetal bovine serum. Neurons were plated onto poly-D-lysine-coated 12-mm glass coverslips at a density of 70,000 cells/cm² for electrophysiological experiments or onto 29-mm glass-bottom dishes (Cellvis) at 18,000 cells/cm² for imaging experiments. Cultures were maintained at 37°C in a humidified incubator containing 5% CO_2.

For imaging experiments, the plating medium was replaced after 3 h with conditioned Neurobasal medium supplemented with 2% B27 and 1% GlutaMAX. For artificial synapse co-culture experiments, medium replacement was performed 24 h after plating. One week later, half of the culture medium was exchanged with conditioned fresh maintenance medium.

Methods

Structural modelling

A near-complete structural model of the human $GABA_AR$ was generated by homology modelling using UCSF ChimeraX (version 1.12). High-resolution structures of the human α1β3γ2L $GABA_AR$ (PDB: 9EQG) were used as templates for model generation. A multiple sequence alignment was constructed using the extracellular, ligand-binding, and transmembrane domains of the α1, β3, and γ2L subunits. The large intracellular M3-M4 cytoplasmic loop was excluded from modelling because this region was absent from the available structural templates. Pentameric receptor models were assembled in the canonical 2α1:2β3:1γ2L stoichiometry with the subunit arrangement β3-α1-β3-α1-γ2L when viewed from the synaptic cleft. Structural models were used to visualise the locations of the epilepsy-associated β3G32R and β3E180G variants within the receptor architecture and to assess their proximity to functionally important structural elements.

Plasmids and molecular biology

Human $GABA_AR$ α1 (pcDNA3.1), α5 (pcDNA3.1Zeo), β3 (pcDNA Zeo), and γ2L (pcDNA3.1) subunit cDNAs were used for expression studies. Human $GABA_AR$ constructs were generously provided by Prof. Neil Harrison (Columbia University). Mouse Neuroligin-2A (Addgene #15259), EGFP (Addgene #13031), pHluorin-tagged β3 (β3-SEP; Addgene #49171, gift from Tija Jacob and Stephen Moss), and gephyrin-mCherry (Addgene #68820, gift from Shiva Tyagarajan) were used throughout the study.

The β3-SEP construct contains a superecliptic pHluorin tag inserted into the extracellular N-terminal domain of the β3 subunit. This modification enables selective visualization of surface-expressed receptors because fluorescence from internalized receptors is largely quenched in acidic intracellular compartments and has previously been shown not to alter receptor trafficking, synaptic targeting, or functional properties [62].

To generate the *wt* β3-SEP construct used in this study, a C283V substitution was introduced into the Addgene β3-SEP plasmid to restore the reference mouse β3 sequence (UniProtKB P63080). Epilepsy-associated β3G32R and β3E180G variants were subsequently generated by site-directed mutagenesis and verified by complete plasmid DNA sequencing prior to experimental use. The following forward primers were used for mutagenesis: C283V, 5′-CCCTTGGGATTACCACCGTGCTCACCATGACAACC-3′; G32R, 5′-GAACGATCCCaGGAACATGTCCTTTGTG-3′; and E180G, 5′-TGCACTTTGGAAATTGAAAGCTATGGCTAC-3′.

Reagents and antibodies

The following primary antibodies were used: rabbit anti-$GABA_AR$ γ2 (Synaptic Systems, Cat. No. 224003), ATTO647N-conjugated anti-GFP antibody (Synaptic Systems, Cat. No. 132003AT1), and Oyster550-conjugated anti-synaptotagmin-1 antibody (Synaptic Systems, Cat. No. 105311). Secondary antibodies included Alexa Fluor 555-conjugated goat anti-rabbit IgG (Thermo Fisher Scientific, Cat. No. A-31572). Diazepam (Sigma-Aldrich) and Gabazine (SR95531; Merck) were obtained from commercial sources and prepared according to manufacturers' recommendations. For single-particle tracking experiments, surface β3SEP-containing receptors were labeled with ATTO647N-conjugated anti-GFP nanobodies (FluoTag-X4, Synaptic Systems, Cat#N0304-AF647-L). Bovine serum albumin (BSA; Sigma-Aldrich) was used in blocking solution and DAPI (Thermo Fisher) for nuclear staining.

The following reagents were used for preparation and maintenance of neuronal cultures: Dulbecco's Modified Eagle Medium (DMEM; Thermo Fisher Scientific), Neurobasal Medium (Thermo Fisher Scientific), B27 Supplement (Thermo Fisher Scientific), GlutaMAX Supplement (Thermo Fisher Scientific), fetal bovine serum (FBS; Thermo Fisher Scientific), penicillin-streptomycin (Thermo Fisher Scientific), phosphate-buffered saline (PBS; Thermo Fisher Scientific), and poly-D-lysine hydrobromide (Sigma-Aldrich). Neuronal transfections were performed using Lipofectamine 2000 (Thermo Fisher Scientific) or calcium phosphate transfection reagents prepared from calcium chloride and HEPES-buffered saline.

Diazepam (Sigma-Aldrich) was used at a final concentration of 1 μM for receptor potentiation experiments. Gabazine (SR95531; Merck) was used at a final concentration of 10 μM for 24 h to chronically block GABAA receptor activity in neuronal cultures.

Artificial synapse preparation

Artificial inhibitory synapses were generated as previously described [31, 32, 61]. HEK293 cells were plated onto 35-mm culture dishes one day before transfection and transfected using the calcium phosphate co-precipitation method. A total of 0.5 μg DNA was used per dish. Cells co-expressed neuroligin-2A to promote formation of inhibitory synaptic contacts with presynaptic terminals of cultured cortical neurons, while EGFP was included to identify transfected cells. HEK293 cells were transfected with α1 or α5, β3, γ2L, neuroligin-2A, and EGFP constructs at a ratio of 1:1:4:1:1 (α:β:γ2L:neuroligin-2A:EGFP) to favour assembly of γ2L-containing receptors. Twenty-four hours after transfection, cells were washed with PBS and plated onto mature cortical neuronal cultures (DIV28-35). Functional artificial synapses typically formed within 24 h of co-culture, and recordings were obtained from co-cultures maintained for up to 4 days

HEK293 surface-expression experiments

For surface-expression measurements, HEK293 cells were transfected using Lipofectamine 2000 and analysed 48 h after transfection. Cells were transfected using the same $GABA_AR$ subunit ratios employed in electrophysiological experiments.

Neuronal transfection and pharmacological treatments

For neuronal imaging experiments, cultured cortical neurons were transfected at DIV10-13 using Lipofectamine 2000. Neurons were co-transfected with β3SEP constructs and gephyrin-mCherry at a DNA ratio of 3:1. For experiments examining receptor distribution and mobility relative to presynaptic terminals, neurons were transfected with β3SEP constructs alone. Active presynaptic boutons were identified immediately before imaging by live labelling with Oyster 550-conjugated anti-synaptotagmin-1 antibodies. Gabazine experiments were performed by treating neuronal cultures with 10 μM Gabazine for 24 h before imaging.

Electrophysiology

Whole-cell recordings

Whole-cell voltage-clamp recordings were obtained from HEK293 cells forming artificial inhibitory synapses with cultured cortical neurons. Recordings were performed at room temperature (23-25°C) using an Axopatch 200B amplifier, Digidata 1440A digitizer, and pCLAMP 11 software (Molecular Devices). Cells were voltage-clamped at −70 mV and currents were low-pass filtered at 5 kHz and digitized at 20 kHz. Only recordings with stable series resistance below 10 MΩ throughout the experiment were included in the analysis. The

membrane capacitance of HEK293 cells was typically ~20 pF, yielding an estimated series resistance–capacitance time constant of approximately 200 µs and a theoretical cutoff frequency in the hundreds of hertz range. Under these conditions, the uncompensated recording configuration was considered acceptable for the purposes of this study, and series resistance compensation was not applied.

Cells were continuously superfused with extracellular solution (ECS) containing (in mM): 140 NaCl, 5 KCl, 2 $CaCl_2$, 1 $MgCl_2$, 10 HEPES and 10 D-glucose, adjusted to pH 7.4 with NaOH. Patch electrodes (4-6 MΩ) were fabricated from fire-polished borosilicate glass capillaries (GC150F-7.5, Harvard Apparatus, MA, USA) and filled with intracellular solution containing (in mM): 145 CsCl, 2 $CaCl_2$, 2 $MgCl_2$, 10 HEPES and 10 EGTA, adjusted to pH 7.4 with CsOH.

Spontaneous inhibitory postsynaptic currents (sIPSCs) were analysed offline using AxoGraph 1.7.6 (AxoGraph Scientific, Australia). Events were detected using a semi-automated template-matching algorithm with a signal-to-noise threshold of 3:1. To exclude overlapping events, all detected currents were visually inspected and only isolated sIPSCs exhibiting a monotonic rise and decay phase were included in subsequent analyses. For each cell, peak amplitude, 10-90% rise time, single-exponential decay time constant, and charge transfer were determined from individual events and averaged to generate a single biological replicate for statistical analysis.

For diazepam modulation experiments, cells were continuously perfused with ECS and spontaneous synaptic activity was recorded for 10 min under control conditions. Diazepam (1 µM) was subsequently applied for 5 min and recordings were repeated from the same cell. Diazepam was delivered by gravity-driven perfusion through a 0.5 mm internal diameter Teflon tube positioned on top of the recorded cell. Switching between control and drug-containing solutions was achieved using a two-way valve upstream of the recording chamber, exposure of surrounding neurons to diazepam was minimal. The solution exchange time was approximately 10 s. Diazepam potentiation was quantified by comparing the mean amplitude, decay kinetics and charge transfer of sIPSCs recorded before and during drug application in the same cell.

Immunocytochemistry and surface receptor measurements

Surface expression of $GABA_AR$ subunits was quantified in HEK293 cells 48 h after transfection. Cells were fixed in 4% paraformaldehyde and 4% sucrose in PBS for 5 min and washed with PBS. All surface-labeling procedures were performed in the absence of detergent

permeabilization to restrict antibody access to extracellular epitopes. Cells were blocked in imaging medium containing 1% BSA for 1 h at room temperature and incubated overnight at 4°C with a rabbit anti-$GABA_AR$ γ2 antibody diluted 1:500 in PBS containing 1% BSA. After washing, cells were incubated for 3 h at room temperature with Alexa Fluor 555-conjugated goat anti-rabbit secondary antibody diluted to 1:1000 in PBS containing 1% BSA. Surface β3-containing receptors were subsequently labelled using an ATTO 647N-conjugated anti-GFP antibody recognizing the extracellular superecliptic pHluorin tag (1:1000 in PBS containing 1% BSA) for 1 h at 37°C.

Following antibody labeling, cells were fixed again for 10 min without permeabilization to preserve surface staining, washed extensively with PBS, and counterstained with DAPI (1 µg/mL in PBS) for 5 min. Coverslips were mounted and imaged under identical acquisition settings within each experimental series.

To exclude potential artefacts arising from steric hindrance, epitope competition, or antibody cross-reactivity between β3 and γ2 labelling protocols, a separate set of experiments was performed in which surface receptor expression was quantified using only the ATTO 647N-conjugated anti-GFP antibody together with DAPI staining. Similar results were obtained under both conditions.

Microscopy

All live-cell imaging experiments were performed at 30°C using an Elyra PS.1 STORM/SIM microscope (Carl Zeiss Microscopy GmbH) equipped with a temperature- and atmosphere-controlled incubation chamber maintained at 5% CO_2 and an Andor iXon Ultra 897 EMCCD camera (Andor Technologies). Images were acquired using ZEISS ZEN Black software (version 2.3 SP1 FP3; Carl Zeiss Microscopy GmbH). A hardware focus-lock system was used throughout all experiments to maintain focal stability during image acquisition.

For single-particle tracking experiments, quantification of gephyrin cluster properties, and analysis of β3SE expression levels in neurons, images were acquired using an α Plan-Apochromat 100×/1.46 NA oil-immersion objective. Measurements of $GABA_AR$ surface expression in HEK293 cells and experiments involving gabazine treatment were performed using a Plan-Apochromat 63×/1.4 NA oil-immersion objective.

Fluorescence detection was achieved using LF488/561-A-000 and LF405/488/561/635-A-000-ZHE beam splitters together with FF01-523/610-25 and FF01-446/510/581/703-25 emission

filters (Semrock, USA) for imaging GFP, mCherry and Alexa Fluor 647 fluorophores. In multicolour experiments, spatial alignment of fluorescence channels was calibrated using fluorescent microspheres (TetraSpeck, 0.2 µm, blue/green/orange/dark red; Thermo Fisher) and corrected using the Channel Alignment module in ZEN software.

Inhibitory synapses were identified by the presence of gephyrin-positive postsynaptic clusters. For experiments requiring identification of all synaptic contacts, including both inhibitory and excitatory synapses, presynaptic terminals were labelled immediately before imaging by live incubation with Oyster 550-conjugated anti-synaptotagmin antibodies (dilution 1:10,000 in imaging medium) for 15 min. For each cell, a minimum of 200 images of synaptotagmin-labelled presynaptic terminals were acquired and averaged to improve signal-to-noise ratio. Only bright, immobile fluorescent puncta were included in subsequent analyses and considered bona fide presynaptic terminals.

For all neuronal imaging experiments, analyses were restricted to perisomatic regions extending 10-60 µm from the cell soma, thereby ensuring consistent sampling of dendritic compartments across cells and experimental conditions.

Single-particle tracking (uPAINT)

Single-particle tracking was performed using universal point accumulation imaging in nanoscale topography (uPAINT). Surface β3SEP-containing receptors were labelled with ATTO 647N-conjugated anti-GFP nanobodies at a final concentration of 300-500 pM for 5 min before imaging. Imaging was performed in extracellular solution supplemented with 10% B27, and equilibrated with 5% CO_2. To reduce non-specific binding, BSA was included in the imaging medium at a final concentration of 0.5%.

Single-molecule image sequences were acquired from neurons expressing *wt* or mutant β3SEP constructs using a 100×/1.46 NA oil-immersion objective. Individual acquisitions consisted of approximately 4,000 frames collected over 2-3 min. To minimise receptor internalisation and maintain neuronal health, imaging sessions were limited to 40 min.

Image analysis

Surface-expression analysis

Fluorescence images were analysed using Fiji/ImageJ [63]. For each field of view, five consecutive image frames were averaged to improve signal-to-noise ratio. Background

fluorescence was removed using local background subtraction (rolling-ball, radius 20 pixels). For analysis of expression levels in HEK293 cells, cell masks were generated using Otsu thresholding and used to identify individual transfected cells. Mean fluorescence intensity for surface-labeled β3 and γ2 subunits was then measured within each mask. For analysis of neuronal β3SE expression, images from at least three consecutive frames were averaged, and a constant background value was subtracted from the entire image. Thresholding was then used to generate selections encompassing neuronal processes, and fluorescence intensities were normalized to the total process length.

Cluster analysis

Analysis of gephyrin clusters was performed following local background subtraction using a rolling-ball radius of 20 pixels to remove diffuse fluorescence arising from out of focus and unclustered gephyrin molecules. Thresholded images were used to generate regions of interest around individual receptor and gephyrin clusters. Cluster number, area, and fluorescence intensity were quantified using the Analyze Particles plugin in Fiji. Synaptic contact density was quantified as the number of gephyrin clusters per unit length of neuronal process, determined by counting gephyrin-positive puncta along manually traced dendritic segments in Fiji.

Single-particle tracking analysis

Single-molecule localization and trajectory reconstruction were performed using the TrackMate plugin in Fiji [64]. Individual molecules were detected using the Laplacian of Gaussian (LoG) detector with sub-pixel localization and median filtering enabled. Trajectories were generated using the Simple LAP tracking algorithm and initially filtered according to trajectory length. Trajectories containing more than 3 localizations were included in localization density analyses. Trajectories comprising more than 10 localizations were used for diffusion coefficient calculations, whereas trajectories containing more than 20 localizations were included in trajectory segmentation analyses.

Synaptic trajectories were identified based on overlap with gephyrin-positive puncta or synaptotagmin-positive presynaptic terminals. Trajectories were classified as synaptic when at least two localizations overlapped with a synaptic mask. Instantaneous diffusion coefficients were determined from a linear fit to the first four points of the mean squared displacement (MSD) versus time lag relationship according to: $MSD(t) = a + 4D\tau$; where D is the diffusion coefficient, a is the y-intercept, and τ is the time lag.

Synaptic receptor mobility was further analysed using divide-and-conquer moment scaling spectrum (DC-MSS) segmentation, adapted from Vega et al [65], to classify receptor motion states and quantify trapping, escape, and dwell-time events. Dwell-time analyses were restricted to complete trapping events consisting of transitions from free diffusion to a trapped state and back to free diffusion. Only trajectories lasting at least 60 frames (1.92 s) were included.

Nanodomain analysis

To quantify receptor surface organization and clustering, single-molecule localizations obtained from TrackMate were further analysed using SR-Tesseler [66]. Voronoï tessellation was used to segment localization maps and identify receptor nanodomains as regions exhibiting localization densities at least two-fold higher than the average density of the corresponding object. Nanodomain area and receptor localization density were calculated from the segmented cluster boundaries and associated localization counts as previously described [66].

Quantification and statistical analysis

Statistical analyses were performed using GraphPad Prism 11 and SigmaPlot 15. No data points were excluded from analysis.

For electrophysiological experiments, measurements from individual synaptic events were averaged within each cell and the resulting value was treated as a biological replicate. For imaging experiments, measurements obtained from individual cells were treated as independent observations. Sample sizes are reported in the figure legends.

Data are presented as mean ± SEM for normally distributed datasets and as median with interquartile range for non-parametric datasets. Normality was assessed before statistical testing. Comparisons among multiple groups were performed using one-way ANOVA followed by Dunnett's multiple-comparisons test or Kruskal-Wallis tests followed by Dunn's multiple-comparisons tests, as appropriate. Pairwise comparisons were performed using two-tailed Student's t tests. Statistical details for individual experiments are reported in the corresponding figure legends. Differences were considered statistically significant at $p < 0.05$.

Acknowledgements

We thank members of the Sah laboratory, Queensland Brain Institute, for helpful discussions and critical feedback on the manuscript. The authors gratefully acknowledge the Queensland

Brain Institute Advanced Microscopy Facility for its support and thank the National Health and Medical Research Council of Australia and the Donald and Joan Wilson Foundation for their financial support of this work.

Statements & Declarations

Funding

This work was supported by the National Health and Medical Research Council of Australia (GNT1147600) and Donald and Joan Wilson foundation to ND.

Competing interests

The authors have no relevant financial or non-financial interests to disclose.

Author Contributions

Nela Durisic, Joe W. Lynch, and Pranesh Padmanabhan conceptualised the study. Material preparation, data collection and analysis were performed by Dejan Gagoski, Edmund Cotter, Li Xu, Justine Haddrill, Jingyi Wu, Vincent Chen, Dubravka Skalamera and Vincent L. Y. Loke. Nela Durisic provided resources, supervision, and funding acquisition. The first draft of the manuscript was written by Nela Durisic, and all authors commented on previous versions of the manuscript. All authors read and approved the final manuscript.

Ethics approval

All animal procedures were approved by the University of Queensland Animal Ethics Committee (approval numbers QBI/142/16/NHMRC/ARC and 2025/AE000100).

Data availability

The datasets generated and analysed during the current study are available from the corresponding author on reasonable request.

Code availability

No custom code was generated for this study.

Figure Legends

Figure 1

Epilepsy-associated GABRB3 variants occupy distinct structural locations within the α1β3γ2 $GABA_AR$

(A) Cryo-electron microscopy structure of the human α1β3γ2L $GABA_AR$ (PDB: 9EQG). The receptor is shown inside and extracellular ("frog's-eye") views to illustrate the spatial arrangement of subunits and the positions of the epilepsy-associated β3 variants. α1 subunits are shown in magenta (~40% opacity), the γ2L subunit in lemon yellow (~40% opacity), and β3 subunits in cyan, with one β3 subunit highlighted. GABA molecules are shown in grey. The receptor is arranged in the canonical β3-α1-β3-α1-γ2L stoichiometry when viewed from the synaptic cleft. The β3G32R variant (orange spheres) is located near the N-terminal region of the extracellular domain, close to the start of the mature protein. In contrast, the β3E180G residue is located within the GABA-binding pocket and lies in direct proximity to bound GABA at the β3+/α1− interface. The side view highlights the pronounced ligand-binding cleft and the proximity of E180 to the neurotransmitter-binding region.

(B) Multiple sequence alignment of $GABA_AR$ β3 orthologues demonstrating that residues G32 and E180 highlighted in orange and maroon, are highly conserved across species. The strong evolutionary conservation of these positions suggests they perform important structural or functional roles and is consistent with the pathogenic effects of the G32R and E180G variants.

Figure 2

β3G32R impairs whereas β3E180G abolishes synaptic currents mediated by α1- and α5-containing $GABA_ARs$.

(A) Representative IPSCs recorded from artificial synapses formed between cortical neurons and HEK293 cells expressing α1β3γ2L, α1β3G32Rγ2L, or α1β3E180Gγ2L receptors. The currents were readily detected in cells expressing *wt* and β3G32R-containing receptors, whereas no detectable synaptic currents were observed in cells expressing β3E180G-containing receptors.

(B) An example of the mean inhibitory synaptic current recorded from a single cell, obtained by averaging the individual events shown in A.

(C) Quantification of IPSC peak amplitude, 10-90% rise time and decay time constant for α1-containing receptors. β3G32R significantly reduced peak current amplitude and accelerated current decay relative to *wt* receptors.

(D) Representative IPSCs recorded from HEK293 cells expressing α5β3γ2L, α5β3G32Rγ2L, or α5β3E180Gγ2L receptors. α5-containing receptors exhibited slower synaptic currents than α1-containing receptors, but the functional effects of the β3 variants were similar.

(E) Example of the mean inhibitory synaptic current from a single cell, calculated by averaging the individual events shown in D.

(F) Quantification of IPSC peak amplitude 10-90% rise time and decay time constant for α5-containing receptors. Like α1-containing receptors, β3G32R decreased current amplitude and accelerated decay kinetics, whereas β3E180G abolished detectable synaptic responses.

Bar plots are mean ± SEM; each data point is an average per cell. n = 10 from individual coverslips in 6 batches of cultures; Unpaired two-tailed Student's t test (WT versus β3G32R), $p < 0.05$; $^{**}p < 0.001$. β3E180G-containing receptors were excluded from kinetic analyses because no detectable IPSCs were observed.

Figure 3

Variants β3G32R and β3E180G do not alter $GABA_AR$ surface expression in HEK293 cells.
(A) Representative immunofluorescence images of a HEK293 cell expressing α1β3E180Gγ2L $GABA_ARs$. The β3 subunit contained an N-terminal SEP. Shown are DAPI-labelled nuclei (blue), total β3-SEP fluorescence (green), surface β3 subunits labelled with an anti-GFP antibody (red), and surface γ2L subunits labelled with an anti-γ2 antibody (magenta). Lower panels show quantification of surface β3 expression in cells expressing α1β3γ2L (left) or α5β3γ2L (right) receptors containing *wt* β3, β3G32R, or β3E180G subunits (box plots showing median, interquartile range, and individual cells). Neither mutation significantly altered surface β3 expression in HEK293 cells.

(B) Representative immunofluorescence images of a HEK293 cell expressing α5β3E180Gγ2L $GABA_ARs$. Shown are total β3-SEP fluorescence (green), surface β3 subunits labelled with an anti-GFP antibody (red), and surface γ2L subunits labelled with an anti-γ2 antibody (magenta). Lower panels show quantification of surface γ2L expression in cells expressing α1β3γ2L (left)

or α5β3γ2L (right) receptors containing *wt* β3, β3G32R, or β3E180G subunits (box plots showing median, interquartile range, and individual cells. Surface γ2L expression was not significantly affected by either mutation.

Kruskal-Wallis, Dunn's test; In (A) n = 100–150 cells per condition from 4 independent cultures, in (B) n = 12–15 cells per condition for α1-containing $GABA_A$Rs and n = 35–38 cells for α5-containing receptors from 3 independent cultures.

Figure 4

Diazepam rescues the function of β3G32R-containing $GABA_A$Rs but not β3E180G-containing receptors

(A) Representative IPSCs recorded from artificial synapses formed between cortical neurons and HEK293 cells expressing α1β3G32Rγ2L or α1β3E180Gγ2L $GABA_A$Rs before (ECS) and after application of 1 μM diazepam (DZ). DZ increased both the amplitude and decay time constant of IPSCs mediated by α1β3G32Rγ2L receptors, whereas no detectable currents were observed in cells expressing α1β3E180Gγ2L receptors under either condition.

(B) Representative IPSCs recorded from HEK293 cells expressing α5β3G32Rγ2L or α5β3E180Gγ2L receptors in ECS and following application of 1 μM DZ. DZ potentiated α5β3G32Rγ2L-mediated currents, increasing both peak amplitude and decay time, whereas β3E180G-containing receptors remained non-functional.

(C) Quantification of DZ-induced changes in peak amplitude for α1β3G32Rγ2L and α5β3G32Rγ2L receptors. Data are normalised to the peak amplitude of the *wt* receptors in ECS. DZ significantly increased IPSC amplitude in both receptor subtypes.

(D) Comparison of charge transfer mediated by α1β3γ2L receptors under control conditions and α1β3G32Rγ2L receptors in the presence of DZ. Both, cumulative probability distributions of charge transfer calculated from individual IPSCs pooled from all recorded cells and mean charge transfer per cell (inset) show that DZ restored chloride flux through α1β3G32Rγ2L receptors to levels indistinguishable from untreated *wt* receptors.

(E) Quantification of DZ-induced changes in IPSC decay time constants mediated by α1β3G32Rγ2L and α5β3G32Rγ2L receptors. DZ significantly prolonged IPSC decay in both receptor subtypes.

(F) Comparison of charge transfer mediated by α5β3γ2L receptors under control conditions and α5β3G32Rγ2L receptors in the presence of DZ. Analysis of pooled event distributions and mean charge transfer per cell (inset) revealed substantial potentiation of α5β3G32Rγ2L receptor-mediated chloride flux by DZ, resulting in charge transfer that was not significantly different from *wt* receptors.

Statistical comparisons between receptor subtypes in (C) and (E) were not performed. In (D) and (F) Unpaired two-tailed Student's t test; $p < 0.05$; *$p < 0.01$; $n = 10$ cells; from individual coverslips in 6 batches of cultures; Bar plots are mean ± SEM.

Figure 5

Epilepsy-associated β3 variants alter gephyrin clustering at inhibitory synapses.

(A) Representative dendritic processes from neurons expressing *wt* β3-SEP, β3G32R-SEP, or β3E180G-SEP (green) together with mCherry-gephyrin (magenta). Merged images are shown in the bottom row.

(B) Quantification of inhibitory synapse density measured from gephyrin-positive puncta. Neither β3G32R nor β3E180G significantly altered the number of inhibitory synapses. Bar plots represent mean ± SEM; each data point is an average per cell; n=20 cells from 8 independent cultures; One-way ANOVA;

(C) Quantification of β3-SEP fluorescence intensity in neuronal processes. Expression of β3E180G was significantly higher than that of *wt* β3 or β3G32R. Boxes represent second and third quartile for each dataset. *$p < 0.05$; Kruskal-Wallis, Dunn's *post hoc*, differences are non-significant; $n = 35$-46 cells per condition from 8 independent cultures.

(D) Analysis of gephyrin cluster properties. Left, cumulative probability distributions of gephyrin cluster area pooled from all analysed synapses, with median cluster area per neuron shown in the inset. Expression of β3E180G shifted the distribution toward smaller values and reduced average cluster area per cell. Right, quantification of gephyrin cluster fluorescence intensity. Both β3G32R and β3E180G reduced gephyrin cluster intensity relative to *wt* β3. Boxes show the interquartile range for each dataset; *$p < 0.05$; **$p < 0.001$; Kruskal-Wallis, Dunn's *post hoc*; left, $n = 1{,}100$-900 synapses, from 30 cells per condition from 8 independent cultures.

(E) Frequency distribution of gephyrin cluster areas. β3E180G produced a pronounced shift toward smaller cluster sizes compared with *wt* β3 and β3G32R. n = 900-1,100 synapses from 30 cells per condition across 8 independent cultures.

(F) Frequency distribution of endogenous gephyrin cluster areas in untreated neurons and neurons treated with Gabazine (10 μM, 24 h). Chronic $GABA_AR$ blockade shifted the distribution toward smaller cluster sizes.

(G) Cumulative probability distributions of endogenous gephyrin cluster area, with mean cluster area per neuron shown in the inset. Gabazine treatment significantly reduced gephyrin cluster area.

(H) Quantification of endogenous gephyrin cluster fluorescence intensity. Chronic Gabazine treatment significantly reduced gephyrin cluster intensity.

(E-H) Untreated, n = 1,000 synapses; Gabazine, n = 600 synapses, from 15 cells per condition across 3 independent cultures. Boxes show the interquartile range. $p < 0.05$, $^*p < 0.001$; Kruskal-Wallis test with Dunn's *post hoc*.

Figure 6. Epilepsy-associated β3 variants differentially alter synaptic $GABA_AR$ mobility and confinement at inhibitory synapses

(A) Representative uPAINT analysis of a neuronal process expressing β3G32R-SEP (green) and gephyrin-mCherry (magenta). The arrow marks an inhibitory synapse. Reconstructed trajectories of individual β3G32R-containing $GABA_ARs$ within the same dendritic segment are shown below. Trajectories within the boxed region were classified as synaptic or extrasynaptic according to their overlap with the gephyrin cluster and are displayed separately beneath the image. The diffraction-limited gephyrin cluster is shown as a black pixelated region.

(B) Synaptic mobility of $GABA_ARs$ containing *wt* β3, β3G32R, or β3E180G subunits. Left, mean squared displacement (MSD) plotted as a function of time lag for all synaptic trajectories. Right, median diffusion coefficients calculated from individual synaptic trajectories. Receptors containing the β3G32R mutation exhibited increased synaptic mobility compared with *wt* receptors, whereas β3E180G-containing receptors displayed reduced mobility.

(C) Example of transient receptor trapping at an inhibitory synapse. Left, representative receptor trajectory showing repeated interactions with a gephyrin-positive synapse. Right,

trajectory segmentation analysis identifies periods of free diffusion (blue), confined diffusion (orange), and immobility (red). This approach was used to quantify receptor exchange between synaptic and extrasynaptic compartments.

(D) Quantification of receptor exchange at inhibitory synapses. The numbers of trapping (▽) and escape (△) events were quantified from segmented trajectories. For all conditions, the numbers of receptors entering and leaving synaptic regions were balanced. β3G32R-containing receptors exhibited significantly higher exchange between synaptic and extrasynaptic regions than *wt* receptors and β3E180G-containing receptors.

(E) Synaptic dwell time analysis. Plot showing the duration of receptor immobilization at inhibitory synapses calculated from complete trapping events. Values represent median dwell times for all synaptic trajectories. β3G32R-containing receptors exhibited significantly shorter synaptic dwell times than *wt* or β3E180G-containing receptors.

(F) Confinement radius of synaptically trapped receptors calculated from confined trajectory segments. Values represent median confinement radii for all synaptic trajectories. β3G32R-containing receptors explored larger synaptic areas than *wt* receptors, whereas β3E180G-containing receptors exhibited the smallest confinement radius, indicating increased spatial restriction within synapses.

Synaptic traces, n = 25,000-22,000 per *wt* or mutant, from 30 cells per condition across 10 independent cultures. Boxes show the interquartile range. $p < 0.05$, $^{*}p < 0.001$; Kruskal-Wallis test with Dunn's *post hoc*.

Figure 7

β3G32R and β3E180G differentially alter synaptic $GABA_AR$ nanoarchitecture

(A) Single-molecule localization analysis of surface $GABA_ARs$. Left, proximal dendrite expressing *wt* β3SE-containing $GABA_ARs$ (green) and gephyrin-mCherry (magenta). The red arrow indicates the region enlarged on the right. The arrows in the inset denote inhibitory synapses. Middle, uPAINT reconstruction of surface β3-containing $GABA_ARs$, with each localization representing the position of an individual receptor. Right, receptor localizations overlaid with gephyrin to distinguish synaptic and extrasynaptic receptor populations. The hollow arrow in the right panel indicates the excitatory synapse shown in (H).

(B) Quantification of total surface and synaptic $GABA_AR$ localizations in neurons expressing *wt* β3, β3G32R, or β3E180G subunits. Although both β3 variants increased surface receptor abundance, synaptic receptor localizations did not increase proportionally. β3G32R-containing receptors were enriched at inhibitory synapses, whereas β3E180G-containing receptors exhibited reduced synaptic localization despite their elevated surface expression.

(C) Representative Voronoï tessellation analysis of synaptic $GABA_AR$ organization. *WT* β3 and β3G32R-containing receptors typically formed large receptor assemblies that occasionally contained receptor nanodomains, whereas β3E180G-containing receptors were more frequently fragmented into multiple smaller receptor clusters. Cluster boundaries are shown in green.

(D) Representative examples of synaptic $GABA_AR$ nanodomains identified by receptor localization density analysis. Examples of synapses containing one, two, three, or more than three nanodomains are shown. Because only β3-containing $GABA_ARs$ were labeled, the total receptor complement present at individual synapses may be underestimated.

(E) Percent of multiple subdomains in the neurons expressing the *wt* β3 or mutant receptors. The proportion of synapses containing multiple nanodomains increased with the severity of receptor dysfunction.

(F) Quantification of receptor localization density within synaptic nanodomains. β3G32R-containing nanodomains exhibited increased receptor packing density compared with *wt* β3, whereas β3E180G-containing nanodomains showed reduced packing density.

(G) Quantification of active synaptic contacts identified by live labeling of presynaptic synaptotagmin-1. Neurons expressing β3E180G exhibited a significant reduction in the number of active synaptic contacts compared with neurons expressing *wt* β3 or β3G32R.

(H) Representative image of a $GABA_AR$ cluster located on a dendritic spine, consistent with an inhibitory synapse on a dually innervated spine. Arrows indicate examples of gephyrin-associated $GABA_AR$ clusters. Arrows indicate examples of DiSs containing β3-positive $GABA_AR$ clusters. Quantification revealed that β3E180G-containing $GABA_ARs$ were detected on DiSs less frequently than *wt* β3- or β3G32R-containing $GABA_ARs$.

n = 30 cells per condition across 10 independent cultures. Bars show mean ± SEM, $p < 0.05$, $*p < 0.001$; One-way ANOVA; Boxes show the interquartile range. $p < 0.05$, $*p < 0.001$; Kruskal-Wallis test with Dunn's *post hoc*.

References

1. Absalom, N.L., et al., *GABA receptors in epilepsy: Elucidating phenotypic divergence through functional analysis of genetic variants.* Journal of Neurochemistry, 2024. **168**(12): p. 3831-3852.
2. Fu, X., et al., *GABA(A) Receptor Variants in Epilepsy*, in *Epilepsy*, S.J. Czuczwar, Editor. 2022: Brisbane (AU).
3. Kan, A.S.H., et al., *Understanding paralogous epilepsy-associated GABA(A) receptor variants: Clinical implications, mechanisms, and potential pitfalls.* Proc Natl Acad Sci U S A, 2024. **121**(50): p. e2413011121.
4. Maljevic, S., et al., *Spectrum of GABAA receptor variants in epilepsy.* Curr Opin Neurol, 2019. **32**(2): p. 183-190.
5. Trevino, M., et al., *Decoding the structural and functional diversity of GABA(A) receptors: from ensemble logic to therapeutic opportunities.* Front Pharmacol, 2025. **16**: p. 1697905.
6. Zhou, J., et al., *Resolving native GABA(A) receptor structures from the human brain.* Nature, 2025. **638**(8050): p. 562-568.
7. Sigel, E. and M.E. Steinmann, *Structure, Function, and Modulation of GABA(A) Receptors.* Journal of Biological Chemistry, 2012. **287**(48): p. 40224-40231.
8. Carricaburu, E., et al., *Gephyrin promotes autonomous assembly and synaptic localization of GABAergic postsynaptic components without presynaptic GABA release.* Proceedings of the National Academy of Sciences of the United States of America, 2024. **121**(26).
9. Olah, S.S., et al., *Acute reorganization of postsynaptic GABAA receptors reveals the functional impact of molecular nanoarchitecture at inhibitory synapses.* Cell Reports, 2023. **42**(11).
10. Pizzarelli, R., et al., *Tuning GABAergic Inhibition: Gephyrin Molecular Organization and Functions.* Neuroscience, 2020. **439**: p. 125-136.
11. Johannesen, K.M., et al., *Structural mapping of variants reveals genotype-phenotype correlations.* Genetics in Medicine, 2022. **24**(3): p. 681-693.
12. Hernandez, C.C. and R.L. Macdonald, *A structural look at GABA(A) receptor mutations linked to epilepsy syndromes.* Brain Res, 2019. **1714**: p. 234-247.
13. Absalom, N.L., et al., *Gain-of-function and loss-of-function variants lead to distinct clinical phenotypes in patients with developmental and epileptic encephalopathies.* Nature Communications, 2022. **13**(1).
14. Menzikov, S.A., S.G. Morozov, and A.A. Kubatiev, *Intricacies of GABAA Receptor Function: The Critical Role of the β3 Subunit in Norm and Pathology.* International Journal of Molecular Sciences, 2021. **22**(3).
15. Pennacchietti, F., et al., *Nanoscale Molecular Reorganization of the Inhibitory Postsynaptic Density Is a Determinant of GABAergic Synaptic Potentiation.* Journal of Neuroscience, 2017. **37**(7): p. 1747-1756.
16. Crosby, K.C., et al., *Nanoscale Subsynaptic Domains Underlie the Organization of the Inhibitory Synapse.* Cell Reports, 2019. **26**(12): p. 3284-+.
17. Gookin, S.E., et al., *Complementary Use of Super-Resolution Imaging Modalities to Study the Nanoscale Architecture of Inhibitory Synapses.* Frontiers in Synaptic Neuroscience, 2022. **14**.
18. Barberis, A., *Postsynaptic plasticity of GABAergic synapses.* Neuropharmacology, 2020. **169**: p. 107643.
19. Maynard, S.A., J. Ranft, and A. Triller, *Quantifying postsynaptic receptor dynamics: insights into synaptic function.* Nat Rev Neurosci, 2023. **24**(1): p. 4-22.
20. Dixon, C.L., et al., *gamma 1-Containing GABA-A Receptors Cluster at Synapses Where they Mediate Slower Synaptic Currents than gamma 2-Containing GABA-A Receptors.* Frontiers in Molecular Neuroscience, 2017. **10**.
21. Nguyen, Q.A. and R.A. Nicoll, *The GABA Receptor β Subunit Is Required for Inhibitory Transmission.* Neuron, 2018. **98**(4): p. 718-+.
22. Brown, L.E., et al., *γ-Aminobutyric Acid Type A (GABA) Receptor Subunits Play a Direct Structural Role in Synaptic Contact Formation via Their N-terminal Extracellular Domains.* Journal of Biological Chemistry, 2016. **291**(27): p. 13926-13942.

23. Cowgill, J., et al., *Structural basis for activation and potentiation in a human α5β3 GABA receptor.* Nature Communications, 2026. **17**(1).
24. Babij, R., et al., *Gabrb3 is required for the functional integration of pyramidal neuron subtypes in the somatosensory cortex.* Neuron, 2023. **111**(2): p. 256-+.
25. DeLorey, T.M., et al., *Somatosensory and sensorimotor consequences associated with the heterozygous disruption of the autism candidate gene, Gabrb3.* Behavioural Brain Research, 2011. **216**(1): p. 36-45.
26. Homanics, G.E., et al., *Mice devoid of gamma-aminobutyrate type A receptor beta 3 subunit have epilepsy, cleft palate, and hypersensitive behavior.* Proceedings of the National Academy of Sciences of the United States of America, 1997. **94**(8): p. 4143-4148.
27. Gurba, K.N., et al., *Mutation, G32R, Associated with Childhood Absence Epilepsy Alters α1β3γ2L γ-Aminobutyric Acid Type A (GABA) Receptor Expression and Channel Gating.* Journal of Biological Chemistry, 2012. **287**(15): p. 12083-12097.
28. Janve, V.S., et al., *Epileptic Encephalopathy De Novo Mutations Impair γ-Aminobutyric Acid Type A Receptor Function.* Annals of Neurology, 2016. **79**(5): p. 806-825.
29. Syed, P., et al., *Effects of GABAA Receptor alpha3 Subunit Epilepsy Mutations on Inhibitory Synaptic Signaling.* Front Mol Neurosci, 2020. **13**: p. 602559.
30. Chen, X., et al., *Inhibitory synapse deficits caused by familial alpha1 GABAA receptor mutations in epilepsy.* Neurobiol Dis, 2017. **108**: p. 213-224.
31. Durisic, N., et al., *SAHA (Vorinostat) Corrects Inhibitory Synaptic Deficits Caused by Missense Epilepsy Mutations to the GABAA Receptor gamma2 Subunit.* Front Mol Neurosci, 2018. **11**: p. 89.
32. Fuchs, C., et al., *GABA(A) receptors can initiate the formation of functional inhibitory GABAergic synapses.* Eur J Neurosci, 2013. **38**(8): p. 3146-58.
33. Leacock, S., et al., *Structure/Function Studies of the alpha4 Subunit Reveal Evolutionary Loss of a GlyR Subtype Involved in Startle and Escape Responses.* Front Mol Neurosci, 2018. **11**: p. 23.
34. Short, B., *Dissecting neurotransmission with artificial synapses.* J Gen Physiol, 2021. **153**(5).
35. Whiting, P.J., *GABA-A receptor subtypes in the brain: a paradigm for CNS drug discovery?* Drug Discov Today, 2003. **8**(10): p. 445-50.
36. Gurba, K.N., et al., *GABRB3 mutation, G32R, associated with childhood absence epilepsy alters alpha1beta3gamma2L gamma-aminobutyric acid type A (GABAA) receptor expression and channel gating.* J Biol Chem, 2012. **287**(15): p. 12083-97.
37. Palpagama, T.H., et al., *GABAA Receptors Are Well Preserved in the Hippocampus of Aged Mice.* eNeuro, 2019. **6**(4).
38. Collinson, N., et al., *Enhanced learning and memory and altered GABAergic synaptic transmission in mice lacking the alpha 5 subunit of the GABAA receptor.* J Neurosci, 2002. **22**(13): p. 5572-80.
39. Prenosil, G.A., et al., *Specific subtypes of GABAA receptors mediate phasic and tonic forms of inhibition in hippocampal pyramidal neurons.* J Neurophysiol, 2006. **96**(2): p. 846-57.
40. Vargas-Caballero, M., et al., *alpha 5 Subunit-containing GABA(A) receptors mediate a slowly decaying inhibitory synaptic current in CA1 pyramidal neurons following Schaffer collateral activation.* Neuropharmacology, 2010. **58**(3): p. 668-675.
41. Zarnowska, E.D., et al., *GABAA receptor alpha5 subunits contribute to GABAA,slow synaptic inhibition in mouse hippocampus.* J Neurophysiol, 2009. **101**(3): p. 1179-91.
42. Absalom, N.L., et al., *Functional genomics of epilepsy-associated mutations in the GABA receptor subunits reveal that one mutation impairs function and two are catastrophic.* Journal of Biological Chemistry, 2019. **294**(15): p. 6157-6171.
43. Tyagarajan, S.K. and J.M. Fritschy, *Gephyrin: a master regulator of neuronal function?* Nature Reviews Neuroscience, 2014. **15**(3): p. 141-156.
44. Ortiz-Lopez, D., et al., *Cryo-EM structures of higher order Gephyrin oligomers reveal principles of inhibitory postsynaptic scaffold organization.* Nat Commun, 2026. **17**(1).
45. Field, M., et al., *Physiological role for GABA(A) receptor desensitization in the induction of long-term potentiation at inhibitory synapses.* Nat Commun, 2021. **12**(1): p. 2112.

46. Groeneweg, F.L., et al., *Gephyrin: a key regulatory protein of inhibitory synapses and beyond.* Histochemistry and Cell Biology, 2018. **150**(5): p. 489-508.
47. Flores, C.E., et al., *Activity-dependent inhibitory synapse remodeling through gephyrin phosphorylation.* Proceedings of the National Academy of Sciences of the United States of America, 2015. **112**(1): p. E65-E72.
48. Battaglia, S., et al., *Activity-Dependent Inhibitory Synapse Scaling Is Determined by Gephyrin Phosphorylation and Subsequent Regulation of GABA(A) Receptor Diffusion.* eNeuro, 2018. **5**(1).
49. Bouthour, W., et al., *A Human Mutation in Associated with Generalized Epilepsy Alters the Membrane Dynamics of GABAA Receptors.* Cerebral Cortex, 2012. **22**(7): p. 1542-1553.
50. Merlaud, Z., et al., *Conformational state-dependent regulation of GABAA receptor diffusion and subsynaptic domains.* iScience, 2022. **25**(11): p. 105467.
51. Zhou, H.X., *Crowding Effects of Membrane Proteins.* Journal of Physical Chemistry B, 2009. **113**(23): p. 7995-8005.
52. Liu, P.G. and P.J. Beltramo, *Effects of crowding on the diffusivity of membrane adhered particles.* Soft Matter, 2023. **19**(40): p. 7708-7716.
53. Kokolaki, M.L., A. Fauquier, and M. Renner, *Molecular Crowding and Diffusion-Capture in Synapses.* Iscience, 2020. **23**(8).
54. Li, T.P., et al., *Protein Crowding within the Postsynaptic Density Can Impede the Escape of Membrane Proteins.* Journal of Neuroscience, 2016. **36**(15): p. 4276-4295.
55. de Luca, E., et al., *Inter-Synaptic Lateral Diffusion of GABAA Receptors Shapes Inhibitory Synaptic Currents.* Neuron, 2017. **95**(1): p. 63-69 e5.
56. Zieger, H.L. and D. Choquet, *Nanoscale synapse organization and dysfunction in neurodevelopmental disorders.* Neurobiology of Disease, 2021. **158**.
57. Gemin, O., et al., *Unique properties of dually innervated dendritic spines in pyramidal neurons of the somatosensory cortex uncovered by 3D correlative light and electron microscopy.* Plos Biology, 2021. **19**(8).
58. Kleinjan, M.S., et al., *Dually innervated dendritic spines develop in the absence of excitatory activity and resist plasticity through tonic inhibitory crosstalk.* Neuron, 2023. **111**(9): p. 1517.
59. Tang, A.H., et al., *A trans-synaptic nanocolumn aligns neurotransmitter release to receptors.* Nature, 2016. **536**(7615): p. 210-4.
60. Richardson, R.J., S. Petrou, and A. Bryson, *Established and emerging GABA(A) receptor pharmacotherapy for epilepsy.* Front Pharmacol, 2024. **15**: p. 1341472.
61. Dixon, C.L., Y. Zhang, and J.W. Lynch, *Generation of Functional Inhibitory Synapses Incorporating Defined Combinations of GABA(A) or Glycine Receptor Subunits.* Front Mol Neurosci, 2015. **8**: p. 80.
62. Jacob, T.C., et al., *Gephyrin regulates the cell surface dynamics of synaptic GABA receptors.* Journal of Neuroscience, 2005. **25**(45): p. 10469-10478.
63. Schindelin, J., et al., *Fiji: an open-source platform for biological-image analysis.* Nat Methods, 2012. **9**(7): p. 676-82.
64. Tinevez, J.Y., et al., *TrackMate: An open and extensible platform for single-particle tracking.* Methods, 2017. **115**: p. 80-90.
65. Vega, A.R., et al., *Multistep Track Segmentation and Motion Classification for Transient Mobility Analysis.* Biophys J, 2018. **114**(5): p. 1018-1025.
66. Levet, F., et al., *SR-Tesseler: a method to segment and quantify localization-based super-resolution microscopy data.* Nat Methods, 2015. **12**(11): p. 1065-71.

Figures:

Figure 1

A

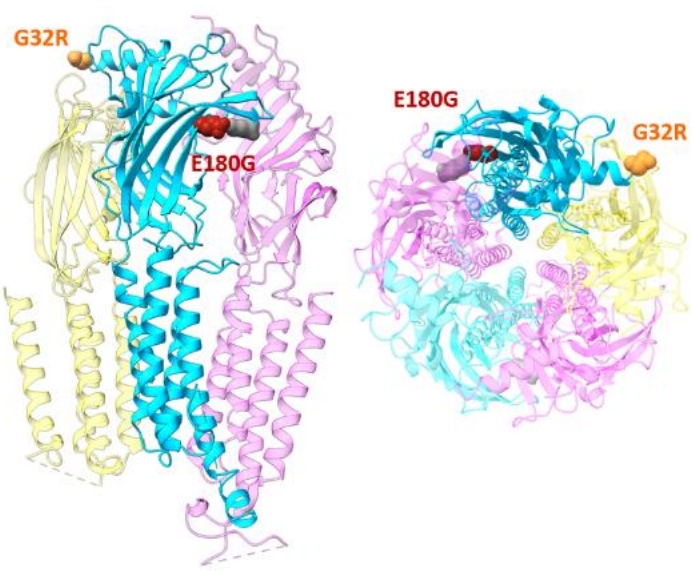

B

	20	30	40
GBRB3_CHICK	GIFSAPVLVA	VVCCAQSVND	PGNMSFVKET
GBRB3_MOUSE	GIFSAPVLVA	VVCCAQSVND	PGNMSFVKET
GBRB3_RAT	GIFSAPVLVA	VVCCAQSVND	PGNMSFVKET
GBRB3_HUMAN	GIFSAPVLVA	VVCCAQSVND	PGNMSFVKET

	170	180	190
GBRB3_CHICK	CMMDLRRYPL	DEQNCTLEIE	SYGYTTDDIE
GBRB3_MOUSE	CMMDLRRYPL	DEQNCTLEIE	SYGYTTDDIE
GBRB3_RAT	CMMDLRRYPL	DEQNCTLEIE	SYGYTTDDIE
GBRB3_HUMAN	CMMDLRRYPL	DEQNCTLEIE	SYGYTTDDIE

Figure 2

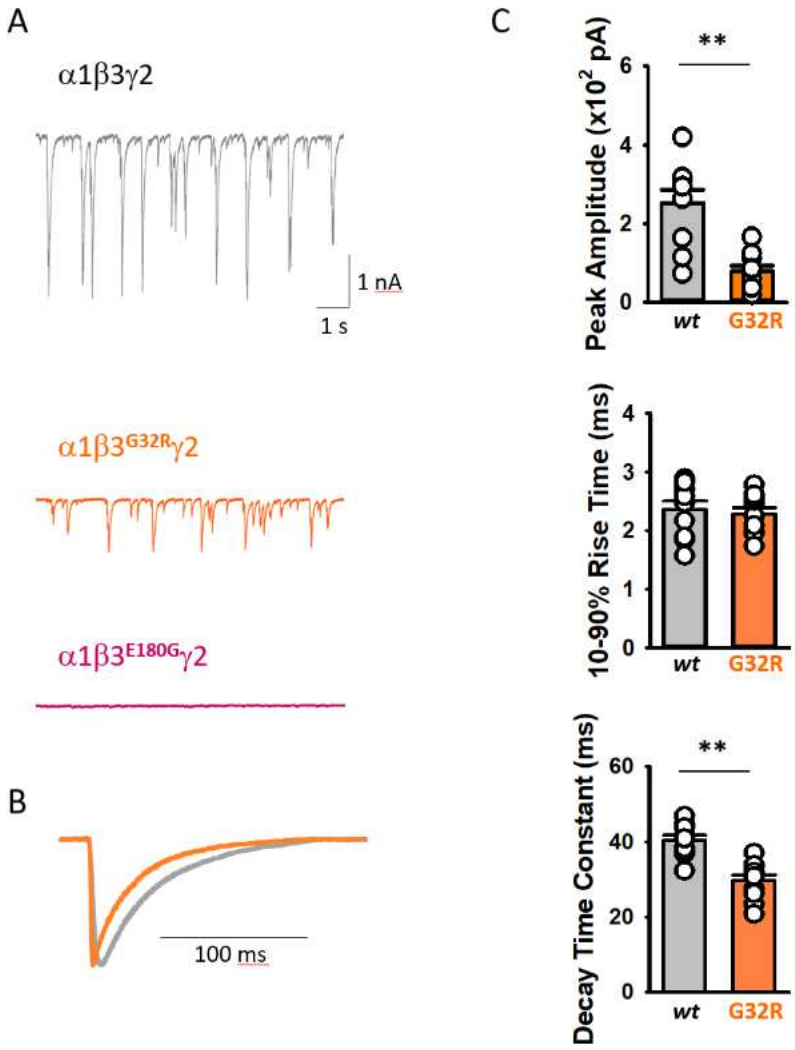

1142

Figure 2

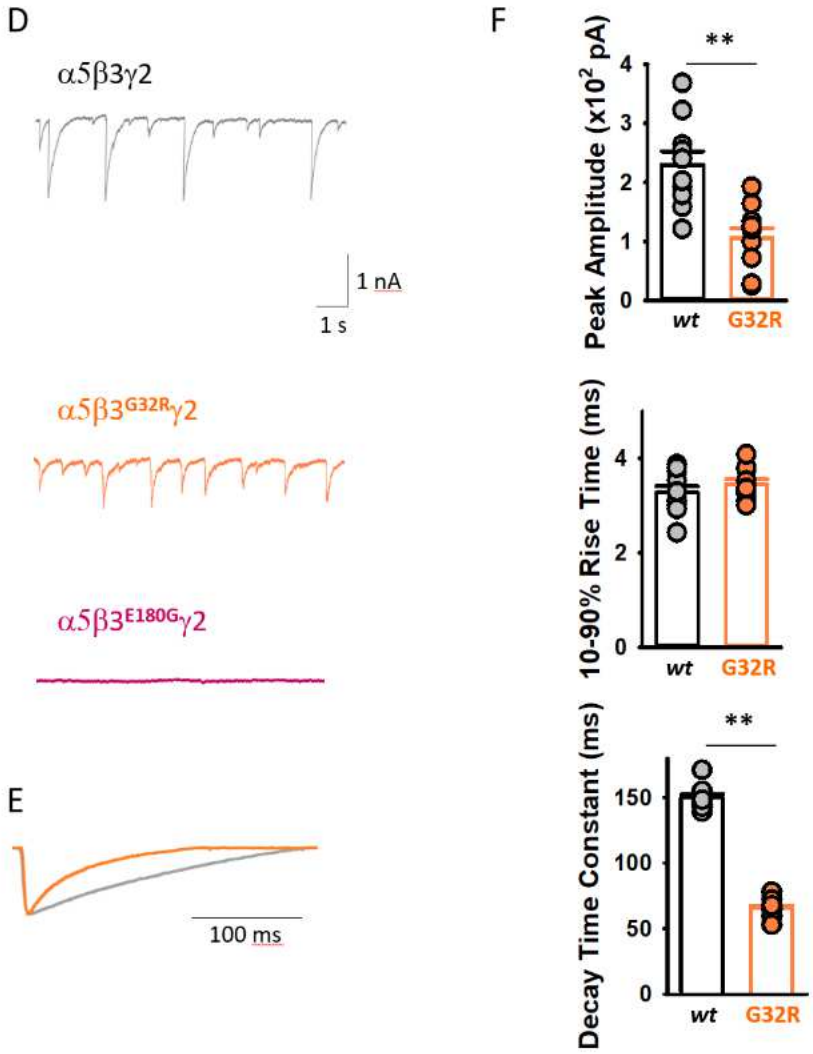

1143

Figure 3

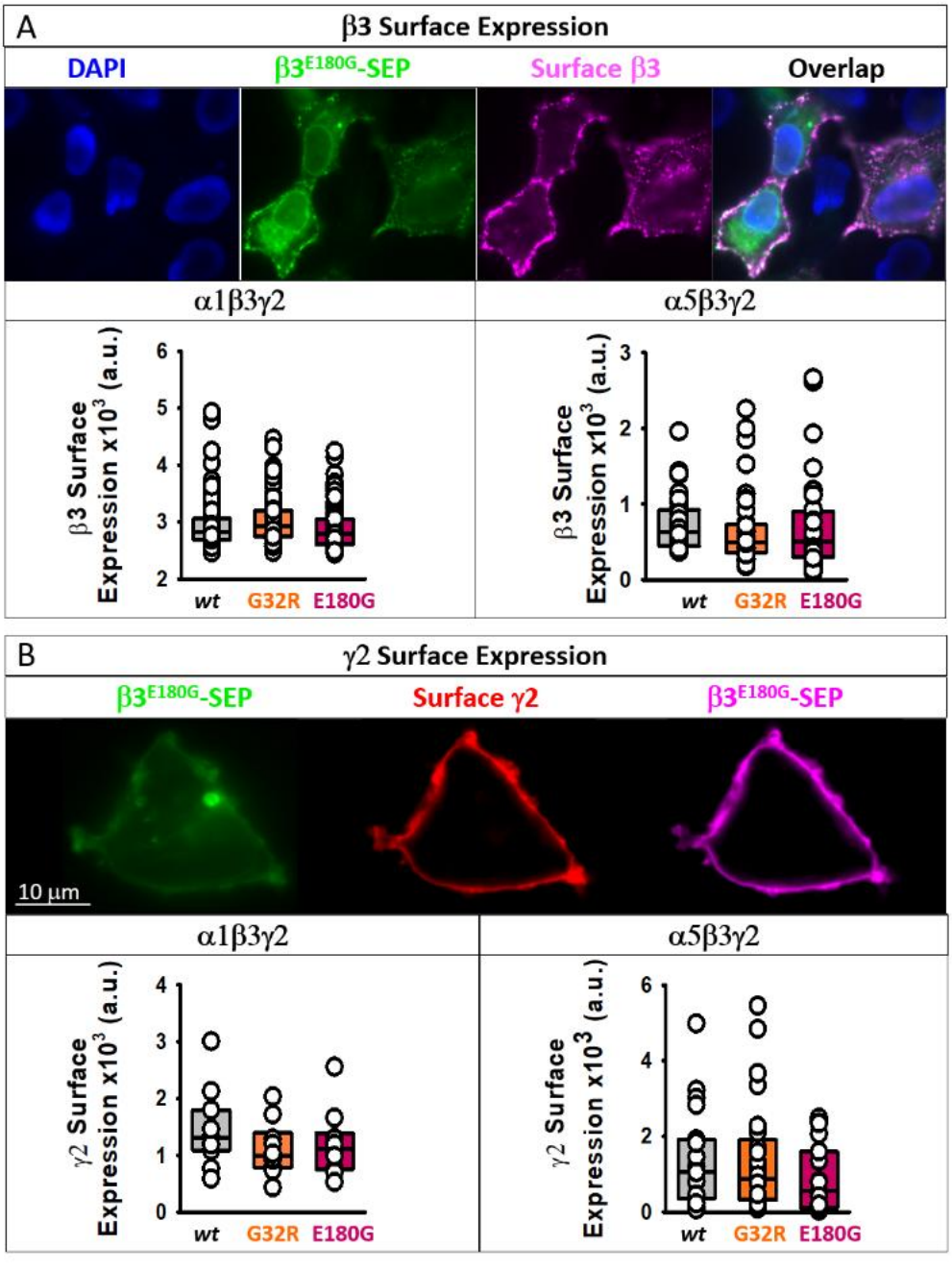

1144

Figure 4

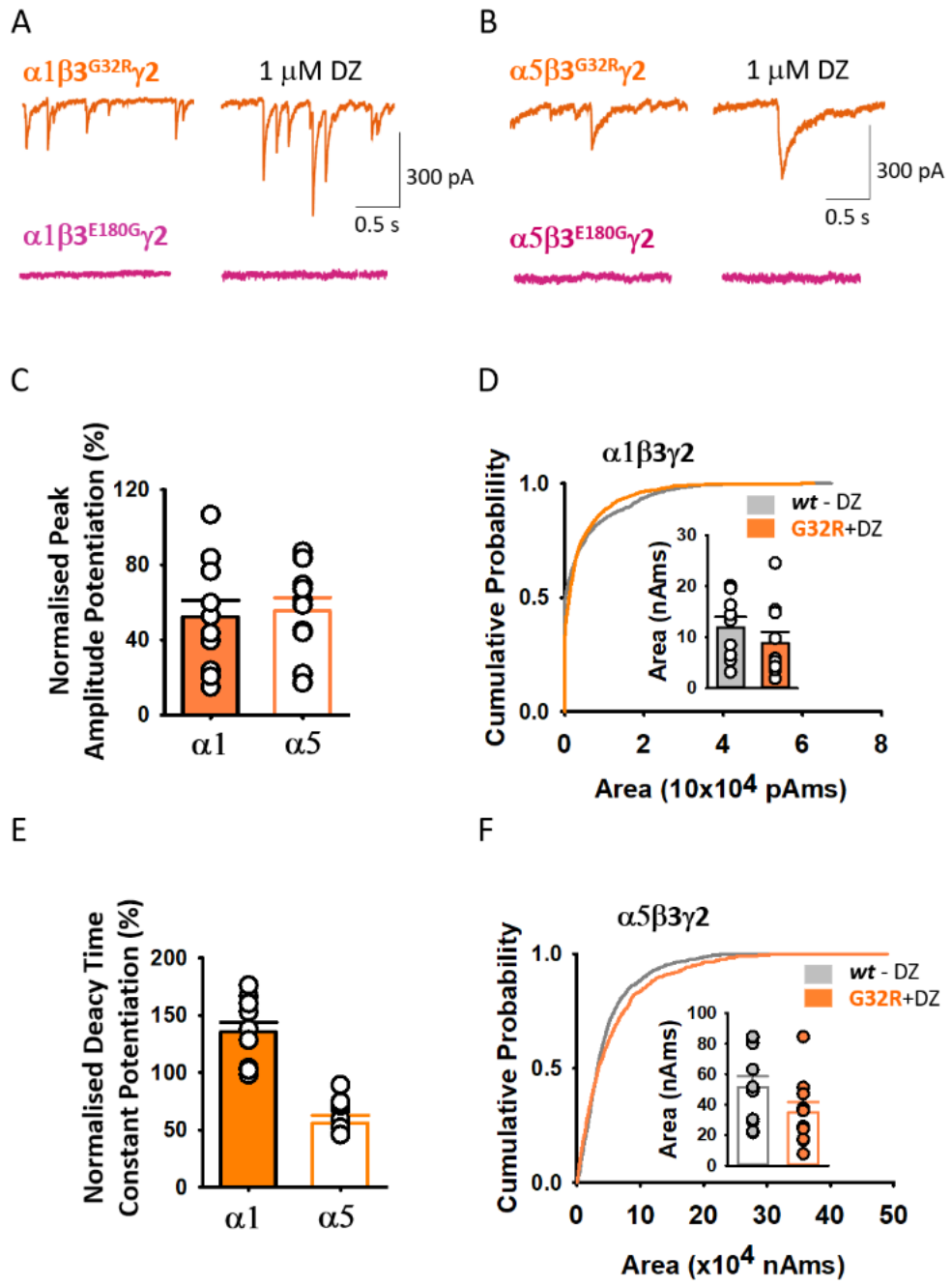

1145

Figure 5

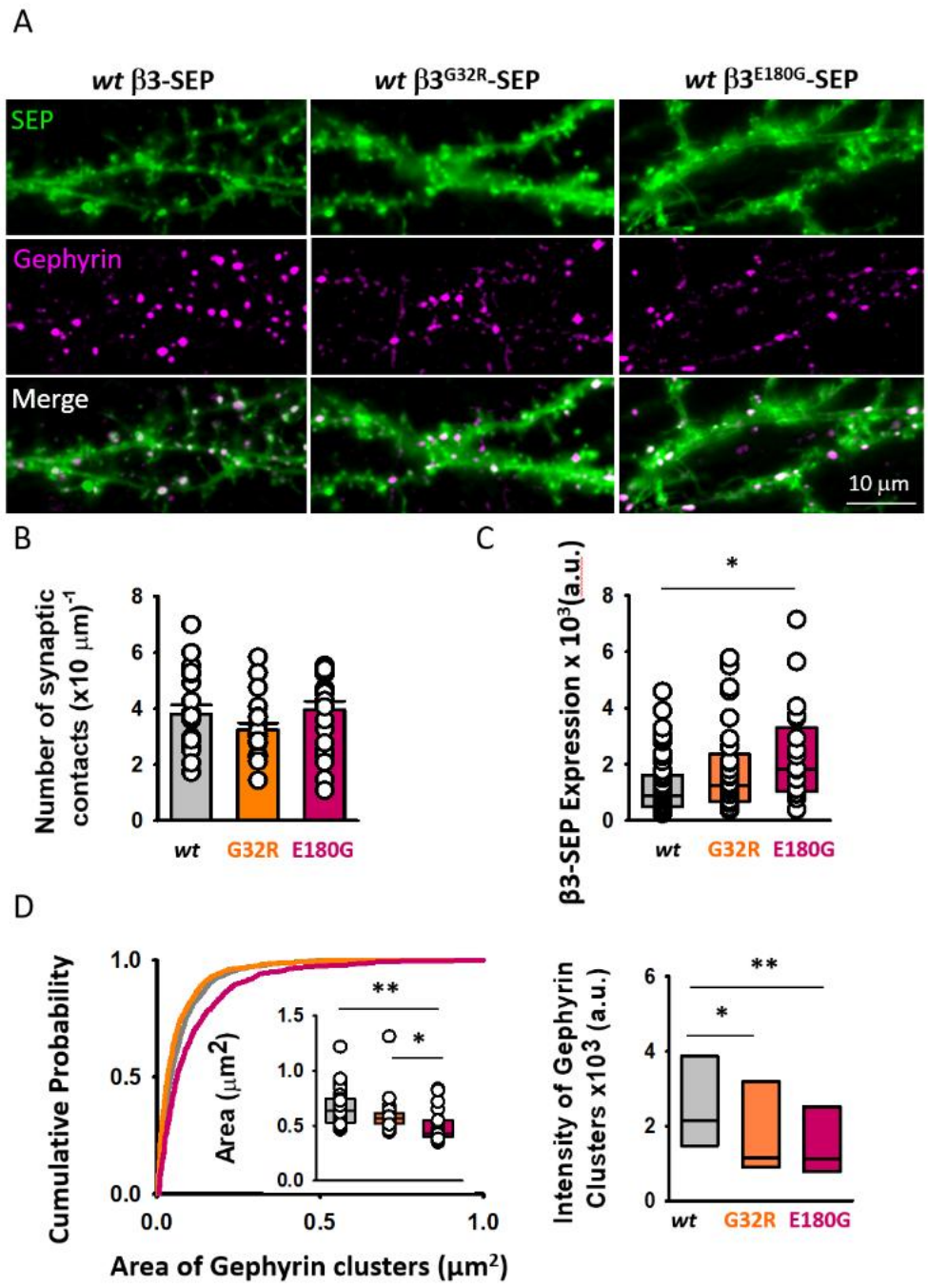

1146

Figure 5

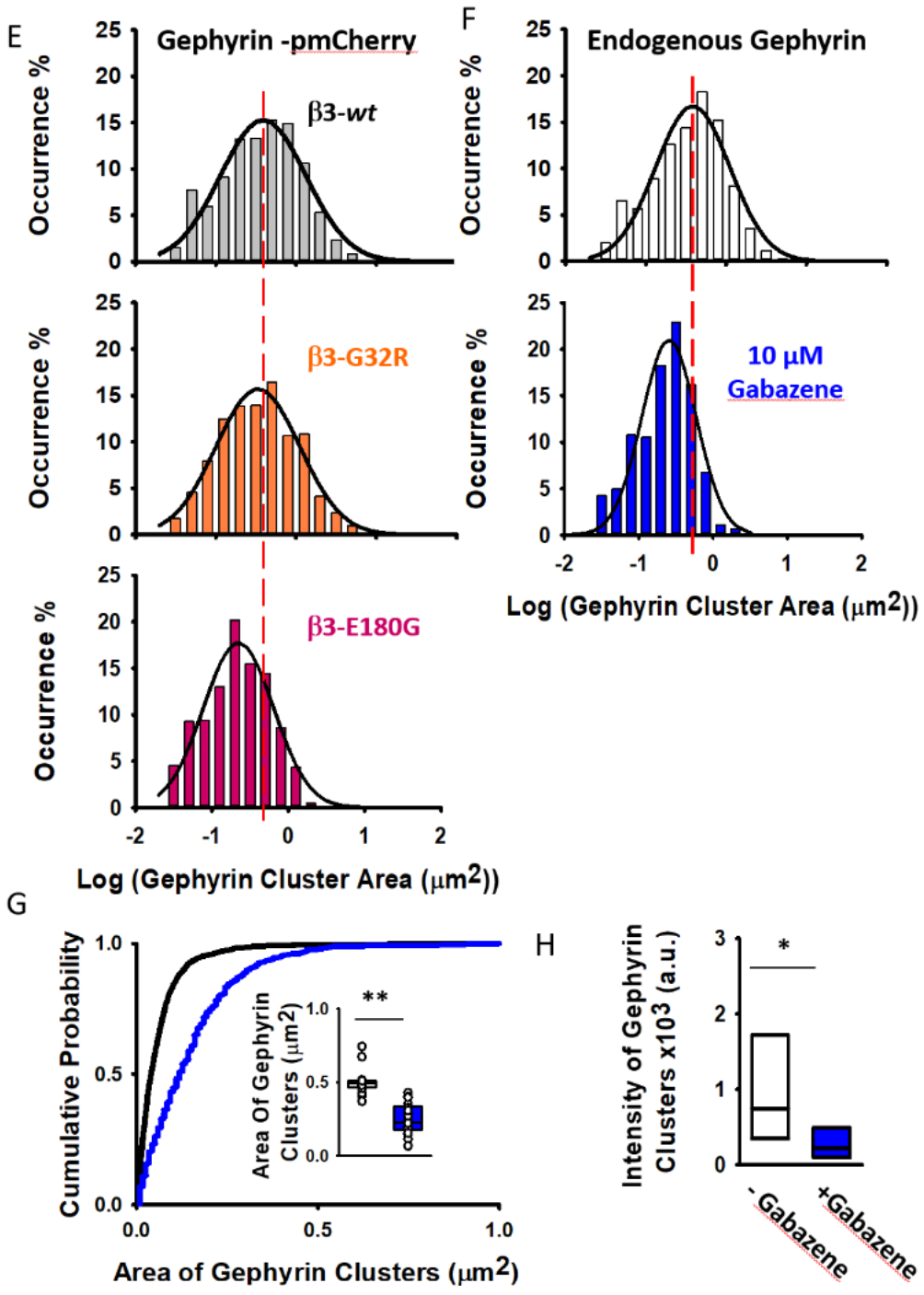

1147

Figure 6

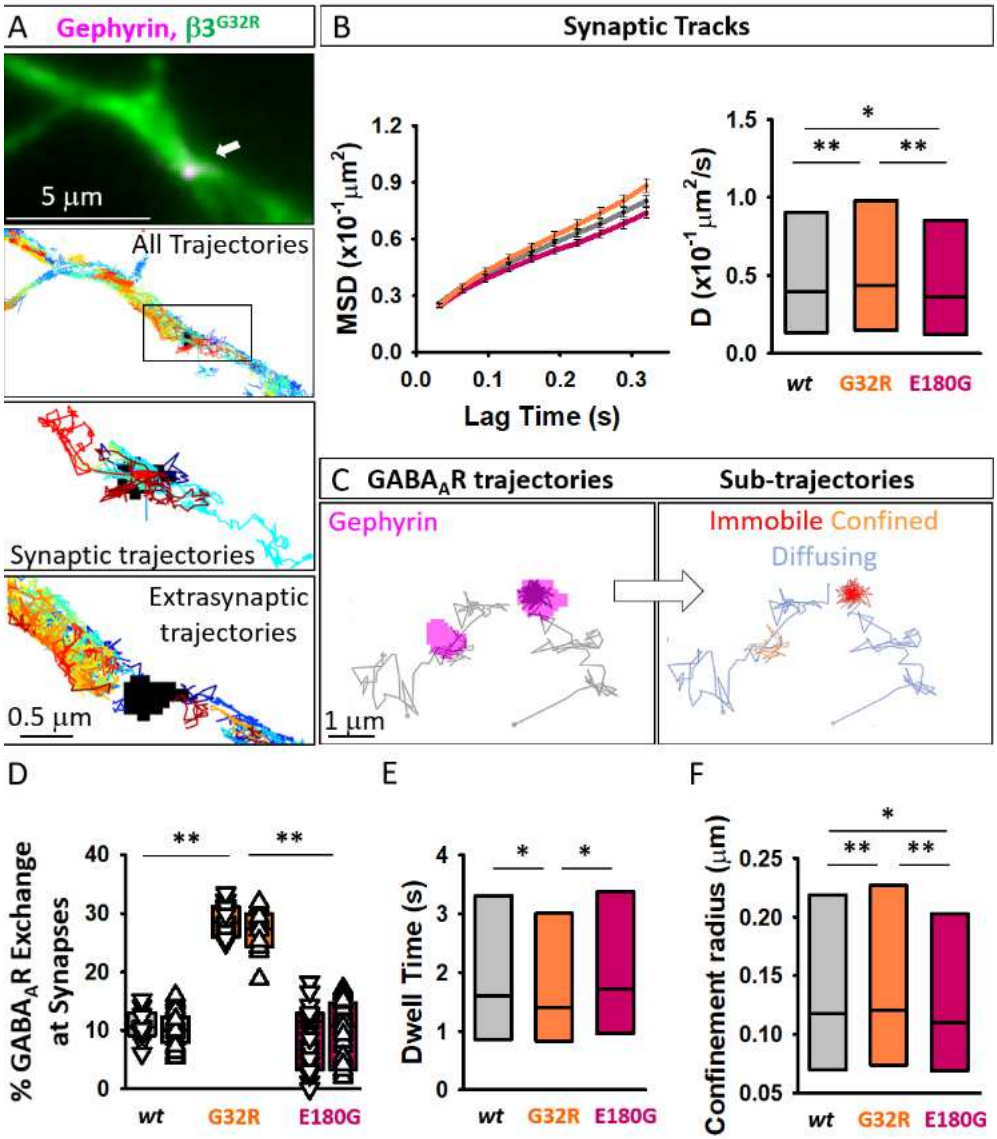

1148

Figure 7

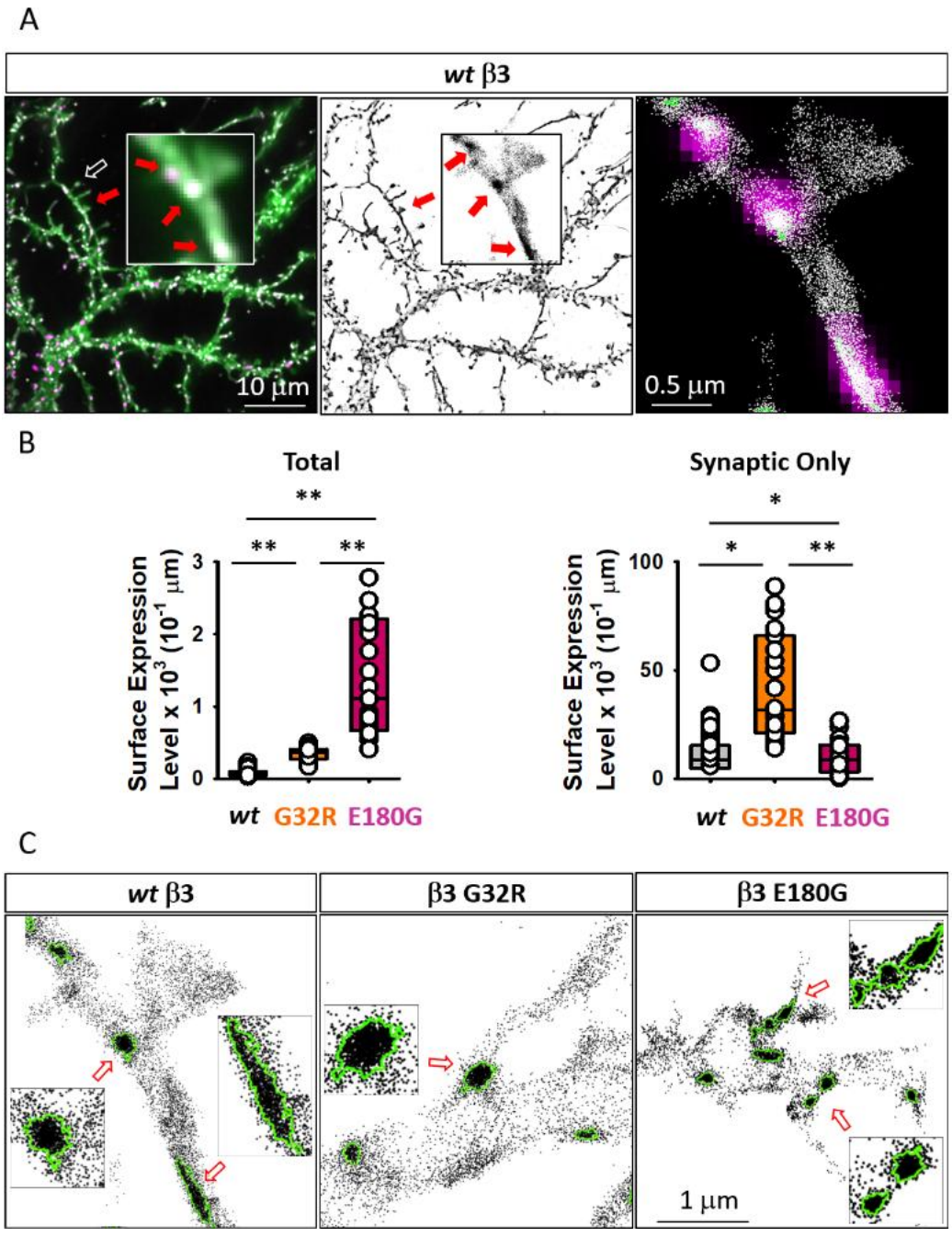
A
wt β3
10 µm
0.5 µm
B
Total
Synaptic Only
Surface Expression Level x 10^3 (10^-1 µm)
wt G32R E180G
C
wt β3
β3 G32R
β3 E180G
1 µm

Figure 7

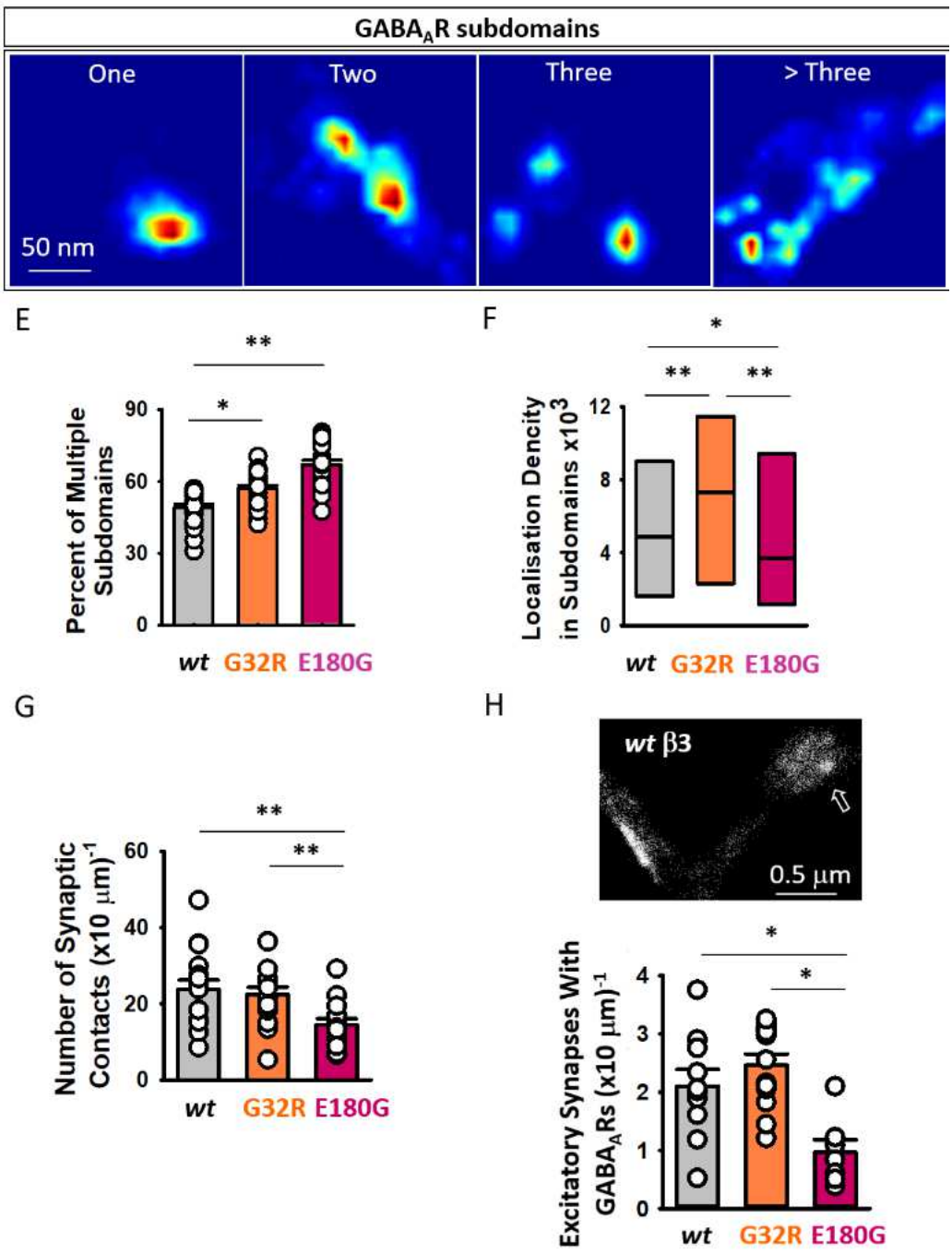

1150

Supplementary Files

This is a list of supplementary files associated with this preprint. Click to download.

- DurisicSupplementalInfo.pdf